1. Blast design management

Maastricht Conference Proceedings 2022, R. Holmberg et al

Blasting a huge overhanging rock formation in an emergency

J. Wallace
Wallace Technical Blasting, Woodland, Washington, USA

W. Gates
McMillen Jacobs Associates, Seattle, Washington, USA

ABSTRACT: On 3 and 10 July 2020, two large sequential rockslides fell near Riggins, Idaho, USA onto highway US-95. It closed the state's only major north-south artery for Idaho, requiring a ten-hour detour to transport personnel, goods, and services. The blast was designed to drop the overhanging rock mass while protecting the remaining backwall, and while keeping the material from spilling into the Little Salmon River just across the highway. All this work took place as emergency work during Covid-19 restrictions and during the time of massive wildfires in the region. Factors critical to project success included Idaho Transportation Department (ITD) engaging experts immediately to address the emergency: a geological engineer with rock engineering experience and Blaster-in-Charge with extensive experience in technical blasting. Blasting was safely and successfully completed on 28 August 2020, the muck pile landed, as designed, out of the river. The project was completed, and the road repaved in November 2020.

1 INTRODUCTION

1.1 Project location

This project is approximately 430 km north of Boise, Idaho, in the Northwest USA.

1.2 Geologic history

On 3 July 2020, a rockslide occurred on a slope along US-95, approximately 5 miles (8 km) south of Riggins, Idaho. The slide narrowly missed vehicles, and the debris-covered highway was closed to traffic. The Idaho Transportation Department (ITD) immediately contacted Bill Gates with McMillen Jacobs Associates (MJA) to assess the failure and provide guidance on reopening the road. Gates' team promptly mobilised a rope-access geotechnical team to assess slope stability and identify key tracking points needed to monitor slope movement. Based on our assessment, US-95 was reopened temporarily using a shoofly to bypass the slide rock debris and under a diligent slope-monitoring protocol. Traffic was limited to daytime only.

This steep canyon along the Salmon River near Riggins is historically prone to rockslides because of the complex structural geology. Rock mass consists of strong hard green serpentinite with weak bands of schist. The slope is about 76 m tall and 244 m long. ITD has reported ravelling and rockslides from this location for over 60 years. Our first time responding to a rockslide on this slope was in December 2012. At that time, MJA established and briefed ITD that the entire slide mass was potentially unstable because of the evidence of large tension fractures between several blocks in the main rock mass, which we identified as Blocks A through D (Figure 2). At the direction of ITD, MJA developed a blasting design that

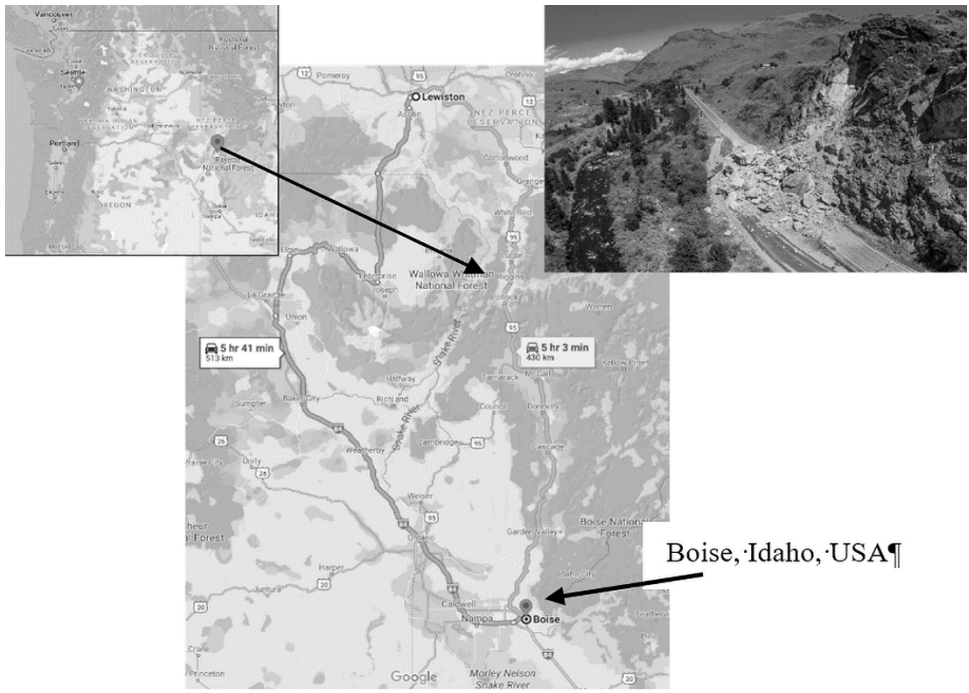

Figure 1. Project location, Riggins rockslide, 10 July 2020, Riggins, Idaho, USA.

allowed quick removal by cushion (trim) blasting of one of the most critical and threatening of the four blocks forming a large-scale wedge on the slope (Block A). The road was reopened to Christmas traffic. After the initial emergency response in 2012, ITD elected to monitor the slope for additional movement. ITD located some survey targets on the rock mass and installed PVC extensometers over the largest tension fracture.

In Figure 2, the left photo shows the rockslide on December 2012, block A removed by trim blasting; middle photo portions of Block C failed on 3 July 2020; right photo rockslide on 10 July 2020, all of blocks B and C and D failed to the tension fracture noted in December 2012 leaving the large rock mass above to be removed by trim blasting.

Eight years later, the investigation of the slope after the July 2020 event revealed the original tension fracture behind Blocks B and D displayed clear evidence of significant opening and movement since 2012. Between 3 July and 8 July, survey data across Block B showed the slope was creeping and the tension fracture was continuing to open. Based on our recommendations, ITD closed the road on July 9. On July 10, Blocks B, D, and the rest of C failed along the tension fracture, fouling the road, exposing the massive underlying wedge failure surface, and leaving a large unstable rock mass in the top throat of the wedge.

The MJA geotechnical field team immediately remobilised to the site to assess the stability of the remaining rock mass of about 12,000+ cubic metres, which weighed approximately 31,232 metric tons. The team instituted slope monitoring and safety protocols. MJA also surveyed the unstable rock slope using our in-house unmanned aerial vehicle (UAV drone) to collect aerial imagery, then ran the data though photogrammetry software to produce topographic plans and slope cross sections for blasting designs, rock anchor layout and drape systems.

Failure occurred along the tension fracture. The unstable upper rock mass was removed by blasting. Note the crushed Connex containers which were used as rockfall barriers. The large boulder above the Connex container is about 10 m high. Together the rockslides dumped about 15,300 cubic metres of rock onto the highway but left a large unstable menacing remnant block of about 12,000+ cubic metres hanging above the highway.

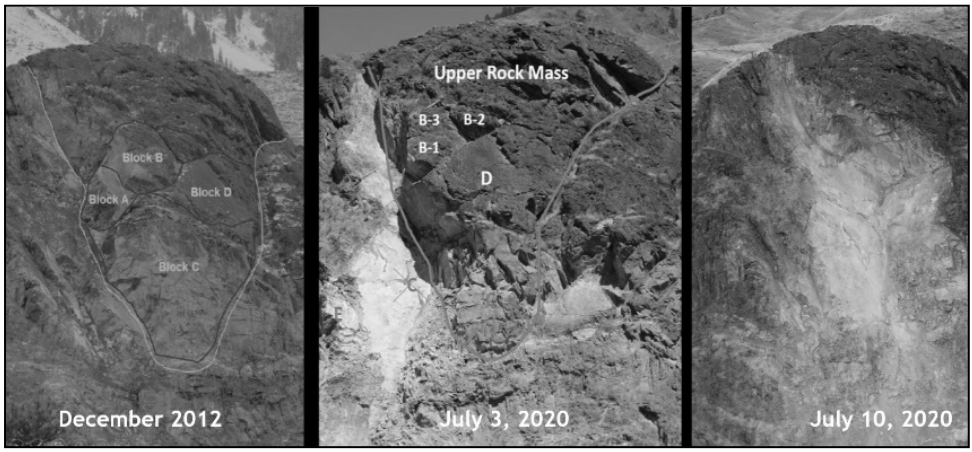

Figure 2. Riggins rockslide sequence of failures.

Figure 3. The third rockslide event on 10 July 2020.

1.3 Monitoring potential movement of the rock mass

Because of the concern for personnel safety working on and below the large unstable rock mass, MJA developed a rigorous monitoring plan to gauge the potential movement of the rock mass. On the 3 and 8 of August 2020, MJA worked with Bridge Diagnostics Incorporated (BDI) and surveyors with David Evans Associates (DEA) to install high-precision slope monitoring telemetry equipment, which included crack (Figure 4). After its installation, field personnel remained to

Figure 4. Installation of instrumentation (crack gauges, tilt meters, prisms) total station targets, extensometers.

monitor the rock mass 24/7. gauges, tilt meters, prisms, extensometers, and survey targets at key locations on the unstable rock mass.

1.4 Naturally occurring asbestos (NOA)

Twenty-one days after the rockslide, ITD advertised the project and conducted a pre-bid meeting to select a contractor. The bid was delayed because naturally occurring asbestos (NOA) was discovered on the rockslope; a first known case of NOA on ITD projects. NOA is different to asbestos associated with building materials. There are several fibrous mineral species, the regulated species include actinolite and tremolite. Non-regulated species include antigorite. Asbestos can cause several forms of cancer. To understand NOA, ITD contracted a subject matter expert (SME) to assess and mitigate the problem. Guided by the SME, MJA established sampling protocol for seven distinct locations on the rockslide scarp (Figure 5). Samples were sent to Asbestos TEM Laboratories of Berkeley, California for identification of potential asbestos mineral species and quantification of the amounts present. Meanwhile, MJA initiated the following mitigation measures: avoid disturbance of areas with suspected NOA, initiate dust control, air monitoring and personnel training. Analytical results demonstrated that NOA was limited to shear zones and schistose areas within the lower zone of the rockslide scarp. Most samples were less than 1% regulated NOA. However, one sample out of the excavation area displayed concentrations of NOA > 5%. The contractor was able to avoid this area and mitigate the large overhanging rock block by drilling and blasting. Lessons learned about NOA: metamorphic greenstones are suspect; NOA is not a project killer.

2 TECHNICAL TRIM BLASTING OF THE LARGE ROCK MASS

Mitigation measures for the rockslide included trim blasting (cushion blasting) of the main rock mass overhang and other associated rock blocks, scaling of loose rock and debris, installation of rock anchor reinforcement, hanging of cable-net-drape and pinned mesh and installation of a

Figure 5. Jim Struthers with MJA using rope access safety techniques sampling for NOA at the contact between the serpentinite rock and the schistose rock units. Photo on the left is a nonregulated fibrous mineral antigorite like the regulated NOA species actinolite and tremolite.

rockfall fence at the toe of the slope in the main fall line.

2.1 Decision to blast

After the emergency assessment of the menacing overhanging block, Gates immediately contacted Jerry Wallace to join the team as the blaster-in-charge. Jerry had a wealth of experience removing similar overhanging rock blocks on other projects. Therefore, the goal was to come up with a blasting plan to remove the large unstable overhanging rock that was threating public safety. It was concluded the best way to remove the threat was by trim blasting in one shot.

Jerry was available but unfortunately his company, Wallace Technical Blasting, Inc., had a contractor's license for private works in Idaho and this project required a public works contractor's license. During the few days it took Jerry to complete the required training and pass the test for the additional license, ITD had the rock in the roadway blasted and removed by a local operator. In the meantime, Gates and crew developed a conceptual blasting plan as a starting point for consideration to remove the block.

The overall contract was awarded on 17 August 2020 to Scarsella Brothers, Inc. of Seattle, Washington for $3 million. Typically, the blaster-in-charge (BIC) and the drilling for the blasting holes would be subcontracted under the general contractor. However, because this was a special

technical blasting problem, Wallace contracted directly to ITD. The hybrid contract meant that the general contractor would be hiring a drilling contractor that could drill to the depths, angle, and hole diameters in the blast plan provided by Wallace as BIC. Ryno Works of McCall, Idaho, was awarded the drilling contract. While exceptionally challenging and on a tight schedule the Ryno Works performed admirably which went a long way to making the blast a success.

2.2 Onsite inspection for blasting

Immediately after acquiring the proper license, Wallace drove to the site and met with Gates and MJA engineering geologist James Struthers. Conversation with a local ITD maintenance personnel indicated that access to the top of the slope was possible via rudimentary roads on the ranch property abutting the top of the slope. Wallace took advantage of that information and went to the top of the slope in the company of the ITD person and evaluated the site, access, and hazards. It was evident that the overhanging rock block would have to be brought down in a single blast. Benching to bring it down in lifts was not feasible and was dangerous because of the unstable conditions. Figure 6 displays the dimensions of the overhanging rock block. Note, the rock block rests on two slide planes that intersected forming a plunge line and a classic wedge for sliding failure.

2.3 Blasting design

After assessing the dimensions of the wedge forming the overhanging rock mass it was established that trim holes would have to be drilled subparallel to the two slide planes to depths exceeding 30 metres. The goal was to release the rock mass from the slide plane and let gravity control the debris slide to the bottom of the slope. Because of the attitude and plunge of the wedge, the left and right trim holes had to be drilled at different depths and angles to avoid running into each other and stay within the rock mass. It was established that production holes would be mostly vertical and shorter than the trim holes, with a single row of angled production holes interspersed between the second row of production holes to pull the broad 'nose' of the mass.

From a safety standpoint, it was ascertained that it would also be necessary to fire the blast as a single trim shot (cushion blast), on short delay timing using electronic detonators, to ensure that the explosives fired in the rock mass while still on the wall rather than while the mass was dropping down the slope. The production holes would be loaded lightly simply to fracture the mass, while the trim row would be hit at about twice the

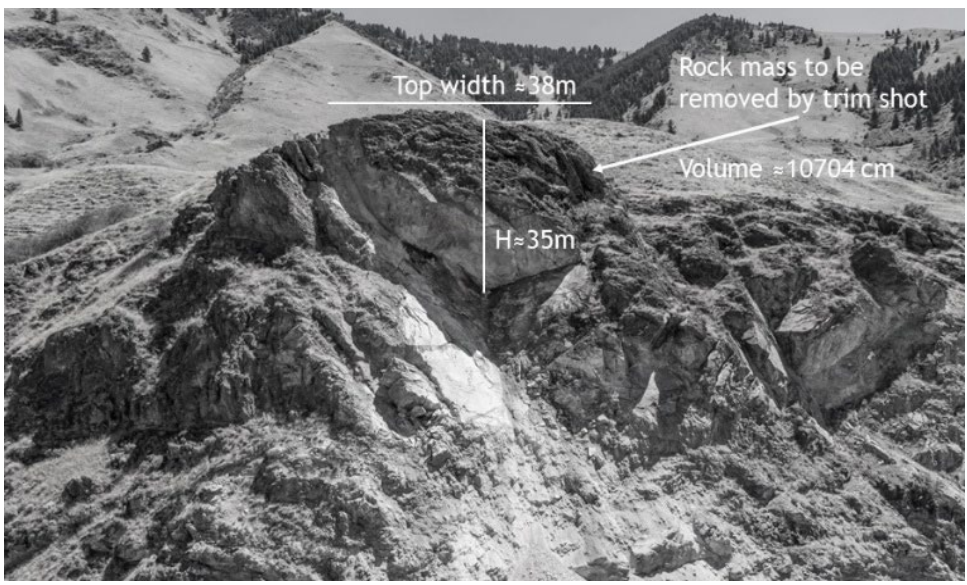

Figure 6. Face view of the 12,000 cubic metre overhanging block, 80 m above the highway, showing the two major angles meeting at the plunge line.

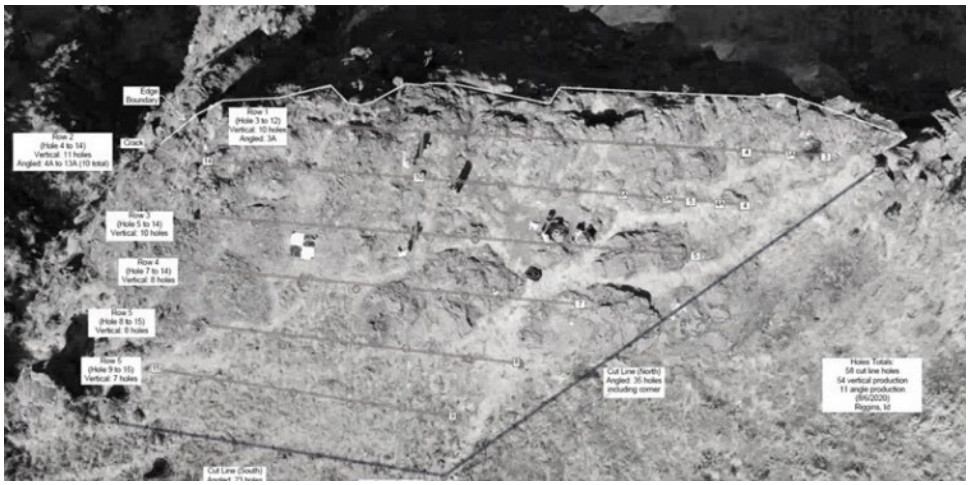

Figure 7. Birds-eye view of production rows and trim rows meeting at the plunge line of the wedge block.

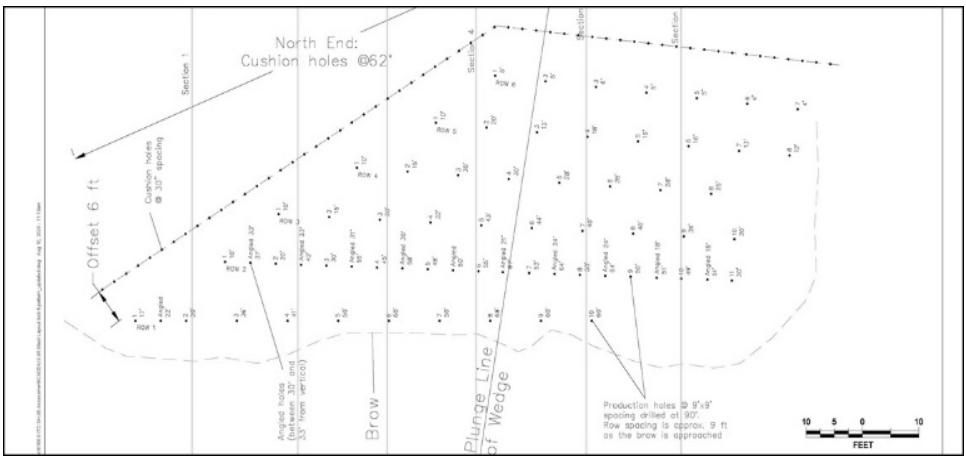

Figure 8. Blasthole layout and angles; angled production holes were drilled between vertical holes in the second row for safety purposes (slope face at the bottom of drawing).

standard trim blast load per square meter of wall to lift the rock off the slide plane and move the material off the wall by gravity sliding.

The final blasting concept was drafted on CAD with the assistance of MJA engineering geologist, Thomas Pallua in the Seattle office in preparation for submittal of the design package to ITD. Preparation of plans and cross-sections were facilitated by using imagery developed by flying a UAV drone. At the same time, Wallace oversaw a ground crew to lay out the blast pattern on the surface of the rock block. Figure 7 displays the blast hole lay out. Figure 8 presents the plan view of the blasting design and Figure 9 displays the cross-sectional view. Figure 10 shows the firing sequence in plan-view.

2.4 Blasting challenges and limitations

The shot design for this large rock block presented several blasting challenges and limitations. For example, we had to remove all the rock material in a single blast because of the instability of formation and lack of future access to a new bench. Because the rock mass was unstable and perched on the slide plane, safety for crew and

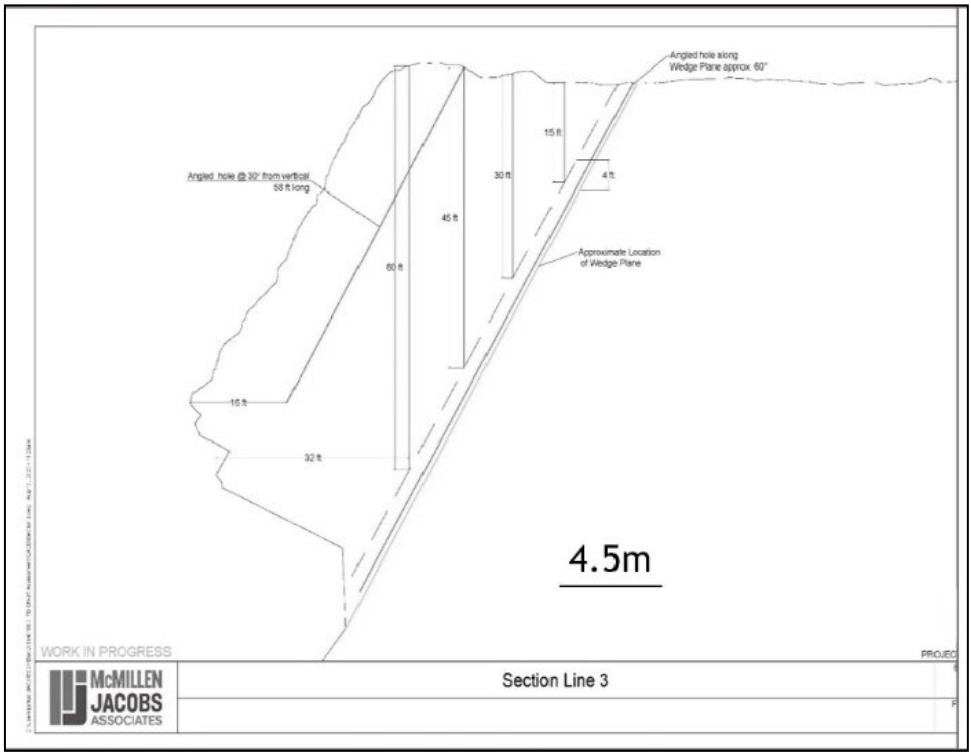

Figure 9. Typical cross-section displaying vertical and angled blastholes sub-parallel to the failure surface.

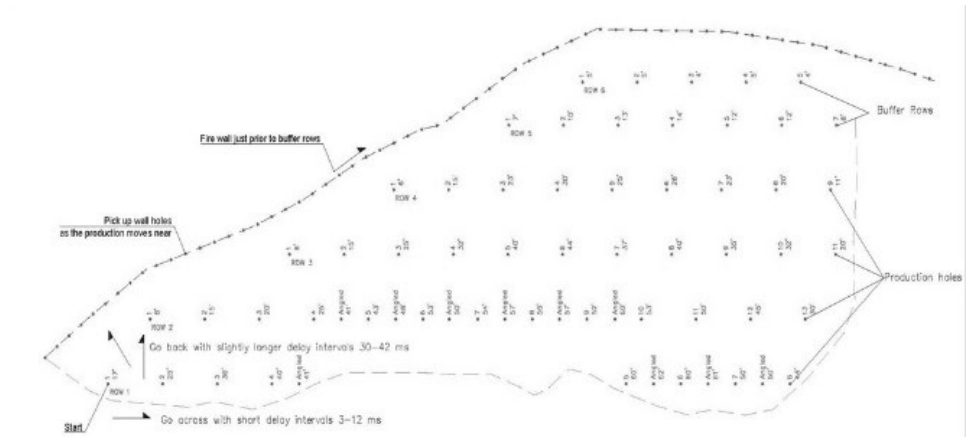

Figure 10. Delay timing showing the 'fast' timing to ensure that the explosives fired within the mass. (Slope face of block is at the bottom of the schematic).

equipment when drilling and loading was paramount. The block was telemetered for early warning of any movement. All equipment was anchored to fixed rock dowels behind the slide plane and fall restraints were provided for the crews. The 29 m perimeter holes along trim line were tough angles to drill and to keep sub-parallel to the failure plane. Moreover, we had to shorten the initiation delay-time to ensure all explosives fired while the rock mass was still on the wall. In

Figure 11. Ryno Works drilling under tough conditions, at 40+C with wildfire smoke filling the horizon. Trim blastholes were drilled at 56 to 60 degrees sub-parallel to the failure surface of the block. Depth of the blastholes were about 30 m.

addition, multiple priming was required for explosive columns over 6 m in length. Finally, we had to keep the blasted rock material from spilling into the Little Salmon River. Figure 11 demonstrates the drilling challenges for this project. Note the drilling rigs are perched out on the overhanging block. All drilling rigs were tied off to a safety bar installed uphill from the block and the rock block was telemetered for potential movement. 130 blastholes were drilled in seven days, with more than half drilled sub-parallel to the failure plane of the block.

2.5 Planning the solution

The solution to the blasting design problem was accomplished as follows: First, fire as a trim shot (post-split, not pre-split design). Shorten the delay timing for firing to ensure all charges fired on the bench or block. Break the production rock without heaving significantly to keep it out of the river. That is, take advantage of gravity. Lightly load the production holes, at near boulder-reduction charge weights, about 15-20% of normal bench blast load. Blast the trim wall with enough energy to move the material slightly, again allowing gravity to take over. The charge weight on trim wall was approximately 0.50 kg per square metre of wall, or roughly double the usual quantity.

2.6 Explosives and loading of the blastholes

Figure 12 displays the typical loading scheme of the trim and production blast holes. Explosives were supplied by a regional major supplier, Northwest Energetic Services located in Deer

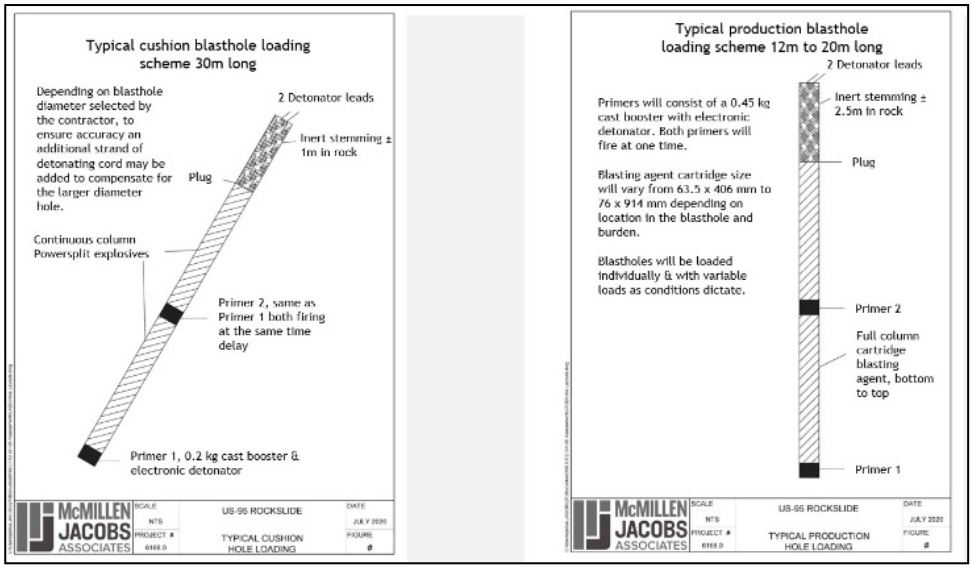

Figure 12. Typical loading scheme for trim (cushion) and production blastholes.

Figure 13. Blasthole loading in progress. Two crews on the trim row at the rear of the block, and one crew on the production holes. Crews on the outer brow of the overhanging rock were tethered off to a safety anchor.

Park, Washington, about a 4 hour drive distant. Loading took one full day. Figures 13 and 14 show the crews loading the blastholes. The crews loaded ±2725 kg of explosives.

The loading of the blastholes, with a minimum of two primers in each hole and with three primers in the long trim holes, took a substantial crew of skilled blasters and helpers. The loading chores were split among three crews, with two crews loading the trim holes. One trim crew was composed of drilling contractor employees, the second composed of employees of the explosive's

Figure 14. The Shot at 1730 hours on 28 August 2020. Note the catchment berms at the toe of the slope.

Figure 15. The image displays the muck pile immediately following the dust clearing from the blast. None of the material ended up in the Little Salmon River, a good success.

supplier. Jerry and his team of MJA helpers loaded the production holes.

The pre-determined delay timing was installed into the electronic detonators and the blast was ready to fire about an hour later than originally scheduled, but well within daylight hours.

2.7 The Shot, 28 August 2020

Once all the blastholes were loaded and ready for firing, the shot was detonated at 1730 hours on 28 August 2020. Maximum explosives per delay was 65.77 kg. Actual peak particle velocity measured at Night Force Ranch (nearest facility) was 2.0 mm/sec. Figure 14 is a photo of the shot and Figure 15 displays the aftermath of the shot. Among other challenges, ITD wanted the shot rock to not end up in the Little Salmon River. A combination of a catchment berm and shoofly at the bottom of the slope coupled with a proper blast design made that possible. Following the large blast on 28 August 2020 another small trim blast further south was fired on 22 September 2020 to close out the blasting work.

Figure 16. Crews loading the production holes at the face of the overhanging rock block. Jerry and Ethan Guzek are tethered to a safety anchor while loading the holes. Alexis Jane with MJA is documenting the explosive loads in real time. James Struthers with MJA is supplying the powder.

3 FINAL SLOPE MITIGATION

Once the rock slope relaxed after blasting (about two days) Scarcella Brothers, the general contractor began removing rock debris to reopen the temporary shoofly road at the toe of the slope. Following the blast, MJA personnel assessed the engineering geology and stability of the blasted slope and the extension of the slope to the south using rope access safety techniques (Figure 16). The teams subdivided the rockslope into zones and identified areas that needed rock scaling, rock anchors or drapes. In addition, plans and drawings were developed to implement the mitigation plans. MJA worked with Rock Supremacy to mitigate the rockslope to accomplish the following: scaling of

Figure 16. Ethan Guzek and Luke Ferguson with MJA assessing the stability of the rockslope using rope access safety techniques after the primary blast on 28 August 2020.

Figure 17. Completed mitigation of the rockslope, rockfall fence and US-95 highway, December 2020.

about 775 cubic metres of rock; drilling and installation of about 1525 metres of rock anchors; installation of 90 metres of drains; installation of 5575 square metres of wire drape; installation of 185 square metres of Tecco Mesh and installation of the rockfall fence. Scarsella Brothers moved about 26750 cubic metres of rock to include the rock berm and repaired US-95. The project was completed on 14 November 2020 except for installation of the rockfall fence which was compete in December of 2020. Figure 17 shows the completed project with the repaired highway, drape on the south end of the slope and rockfall fence at the base of the slope.

4 CHALLENGES AND LESSONS-LEARNED

This was a very intense and challenging project. The emergency required highspeed turnaround of designs and the designs changed on a continuing basis. Use of drone imagery was key to assessing and mapping the rockslope and developing plan sheets and cross-sections for the blasting, anchorage, and drape designs. Monitoring stability of rockslope with telemetry, survey locations and visual observation was key to tracking the potential movement of menacing block. These observations acted as early warning for protecting the workers on the drilling rigs and for closing the road to protect the public. One large trim blast was key to safely removing large unstable rock block. And finally, naturally occurring asbestos (NOA) can create a challenge to the project, but NOA is not a project killer.

5 CONCLUSIONS

Several factors were critical to project success.

First, Idaho Transportation Department (ITD), the Owner, engaged a qualified geotechnical company involved from the start to ensure that the geology of the rock mass was characterised employing special safety equipment and techniques, properly instrumented and stable enough to allow for the work to be accomplished on the rock block and for traffic to flow below.

Second, ITD required a qualified blasting contractor to perform the design, management of drilling and performance of the critical blasting.

Third, ITD awarded the general contract to a highly qualified company who managed and conducted all the other operations, and who worked efficiently with the blasting contractor, the civil and geotechnical engineer.

Fourth, naturally occurring asbestos (NOS) was dealt with, but it was not a project killer.

The blasting was safely and successfully accomplished through the efforts of all involved, including keeping the muck pile out of the river. Cleaning up the rock slope after the shot involved rock scaling, installation of rock anchors and cable net drape. Once completed the highway alignment was corrected and paving completed just prior to winter 2020.

The Owner, Idaho Transportation Department, and the general contractor, Scarsella Bros, along with WTB and MJA, were recently honored with a Top Gold Award for Partnering on this challenging project.

6 RECOMMENDATIONS

When working with unique challenges it is important to have a team made up of experts in all the fields that comprise the challenges. Geotechnical engineering and environmental firms, excavation contractors, scaling and bolting contractors, drilling contractors, and blasting contractors all played significant roles in making this a successful response to a rockfall emergency.

7 ACKNOWLEDGEMENTS

We extend thanks to following companies and personnel that were associated with this very challenging project:

Asbestos TEM Laboratories, Inc.-Mark Bailey

Bridge Diagnostics Incorporated (BDI)

David Evans and Associates, Inc.-Duffy Haggarty and Darrel Ramus

Erskine Environmental Consulting-Dr. Erskine

McMillen Jacobs – Wm. Gates, Jim Struthers, Jamie Schick, Ethan Guzek, Luke Ferguson, Alexis Judy, Justin Reeves, Carol Ravano, Thomas Pallua

HDR, Inc.-Ty Bardwell and Dustin Lenz

Wallace Technical Blasting-Jerry Wallace

Scarsella Brothers Inc.

Rock Supremacy – Rowen Anderegg and crew

Ryno Works – Ryan Miller and crew

WHPacific, Inc. (now NV5) -Jeremy Robbins and Dawson Sigman

Idaho Transportation Department-Dan McElhinney, Doral Hoff, Jared Hopkins, Janet Zarate, Brian Bannon, Bud Converse, Megan Sausser, Mel Moore, D2 and D3 Operations staff

Maastricht Conference Proceedings 2022, R. Holmberg et al

Blast vibration optimisation at a limestone quarry by using E*STAR electronic detonators and advanced modelling methods

V. Kala & E. Kubat
Austin Detonator s.r.o., Vsetin, Czech Republic

ABSTRACT: This paper presents a modern blasting approach based on a combination of advanced software technologies and E*STAR electronic initiation system. A unique geomorphological phenomenon, historical Koněprusy caves, are situated in Central Bohemia, and in close proximity to one of the biggest quarries in the Czech Republic, Čertovy schody. To protect the historical caves and their ecosystems, the ground vibration limits for blasting were set and the stationary vibration monitoring devices were placed inside the caves. Non-electric detonators were used but vibration results were unpredictable due to slight timing inaccuracies, fixed delay times, and no vibration analysis. The innovative blast optimisation software is used to achieve vibration goals as well as to keep the production balance. Since that time, every single blast has been analysed in detail, and the optimum solution for PPV a PVS reduction is chosen. Among the major advantages of a complete process was the accuracy and timing variability of E*STAR detonators.

1 INTRODUCTION

1.1 Location and History

In the 1950s, started the investment plans of building the limestone processing plant 'Vápenka Čertovy schody a.s.' and the quarry 'Čertovy schody'. The quarry and the processing plant are near the city of Beroun, approximately 40 km southwest of Prague (Figure 1).

Since 1962, the processing plant and the quarry have been in full operation. The production initially took place in a quarry opened at the site of the so-called 'Císařský' (today known as a quarry 'Čertovy schody west'). At the end of the 1970s, an opening project for the eastern part of the quarry was created, and production started in 1987. The Koněprusy deposit consists of high-quality limestones with a density of 2.6 – 2.71 g/cm^3. Limestone products are mostly used for agriculture, as building stone, disinfectant, etc. So far, this is one of the largest limestone quarries in the Czech Republic. The average yearly production of limestone products is approximately 2 million tons.

1.2 Koněprusy Caves

Koněprusy Caves are a cave system in the heart of the limestone region known as Bohemian Karst. The name derives from the nearby village of Koněprusy. With a length of 2 km and a vertical range of 70 m, it is the largest cave system in Bohemia. Golden Horse hill conceals the most extensive cave system in Bohemia, which was accidentally discovered after the blasting in a nearby limestone quarry in 1950, and subsequently was made accessible for the public in 1959. The blasting times at the quarry are set on the exact hour, which highly depends on the guided tours for visitors, which are available every day from April to November.

Figure 1. Location of the quarry.

1.3 Blasting Issues

The problems with the blast vibrations started in 2014 when the vibration limits were set to a maximum of 3 mm/s. The caves are approximately 300 m away from the west part of the quarry, and as a result, the quarry management had a significant issue to consider. Various blasting parameters were applied to solve the problem, including non-electric detonators in combination with multi-decking, but without any meaningful improvement.

2 TRANSITION TO ELECTRONIC INITIATION

At the beginning of 2015, the decision was made to try out electronic detonators from Austin Powder. The most important advantages of the E*STAR electronic detonators compared to non-electric detonators are high accuracy, delay range from 1 – 20,000 ms, minimum delay increment of 1 ms, reliability as well as multi-level detonator verification prior to each blast.

2.1 Initial Plan

Before we made any initial plan for the E*STAR blasts, a detailed analysis of the previous non-electric blasts was completed. The most important blasting parameters as well as the vibration results were taken into account. The following table represents the short summary of the non-electric blasts (Table 1).

Table 1. Non-electric blasts analysis.

	Non-electric blasts	E*STAR
Number of blasts	22	-
Benches	300, 320, 338	-
Average exp. per interval	13.25 kg	-
Distance to caves	346 m	-
Average PPV	2.6 mm/s	-
PPV Range	1.1 – 4.1 mm/s	-
% of blast >= 3 mm/s	50%	-

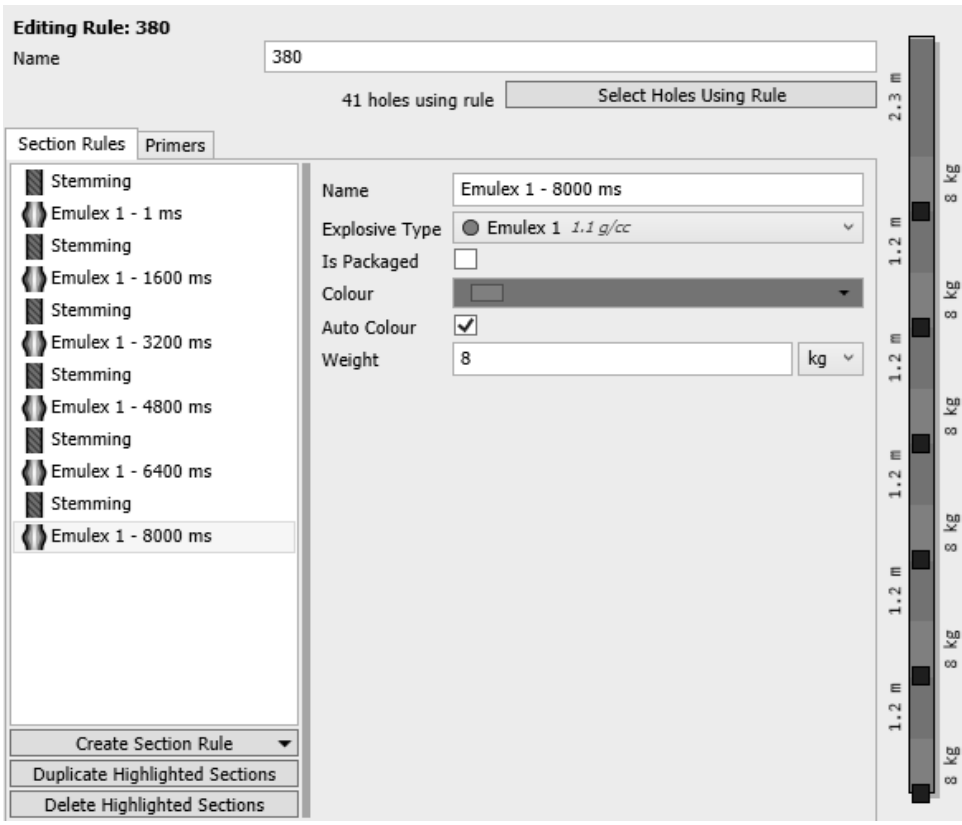

Figure 2. Signature hole parameters.

According to the initial plan, the first step in a blast vibration analysis is to obtain as much information as possible about the local conditions, the rock characteristics, surrounding geology, and the propagation characteristics of seismic waves. After detailed analysis, the charging plan combined with the optimum delay times were applied to the first electronic blast. That would make a proper foundation for the systematic optimisation, where K and n factors were going to be adjusted depending on the blast results.

2.2 Signature Hole

By shooting a single representative borehole (Figure 2), a signature waveform can be isolated for each deck and analysed. Multiple signature holes were blasted on different bench levels. Signature hole parameters (number of decks, stemming, a charge per deck, etc.) were different depending on the bench characteristics, except the diameter, which was 92 mm.

GPS position of each signature hole was measured together with the GPS position of seismographs in the caves. Packaged cartridge explosives were used for the charging, and the stemming material was gravel (Figure 3). The signature holes were blasted individually, so each hole was analysed separately based on the hole parameters and the vibrations waveform.

2.3 Paradigm (Blasting Solutions)

Blasting Solutions analytical tools were the foundation of the Paradigm, state-of-the-art blast optimisation software, which is an essential tool used to enhance the successful design and execution of each blast. Rock properties analysis and geology-based attribute adjustments provide the basis for vibrations optimisation modelling.

By importing the seed wave (Figure 4), exact GPS positions of the signature hole and seismograph, and blast parameters with holes GPS positions, the software is calculating the ideal

Figure 3. Signature hole prior to shot.

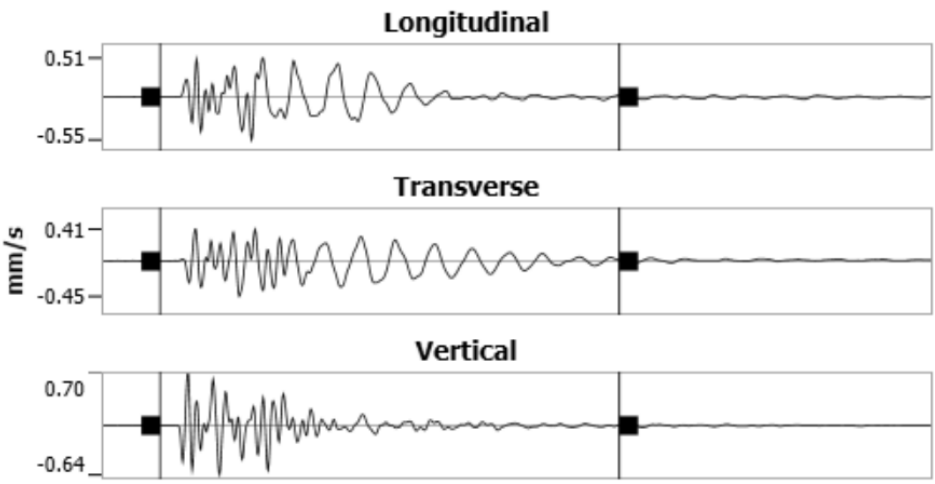

Figure 4. Seedwave attributes.

timings to achieve the lowest seismic impact for the environment and the critical zones. Thousands of combinations allow users to choose the optimum delay times based on preferences.

PPV, PVS, frequencies, perception index, and total blast duration are justsome of the parameters which are taken into account before the final decision.

3 OPTIMISATION

3.1 First results

Before each analysis, the GPS positions of each blast hole were measured and imported to the blast optimising software. After analysing the signature holes results, the optimum delay time was chosen based on the software solutions and experience of the blasters.

In the beginning, to keep continuity and to not make so many changes, the first optimized blasts utilised the same charging parameters as well as number of decks as were blasted with previous non-electric blasts. Only delay times were changed. The average delay between two decks in the single hole was between 11 – 13 ms, with an average inter-hole delay around 120 ms, all with single row blasts.

After the first couple of blasts, the results were more than satisfying (Figure 5). With 5-7 decks per hole, 7.5 – 9 kg of explosives per interval the average PPV was reduced to 1.09 mm/s (values ranged from 0.97 mm/s to 1.30 mm/s).

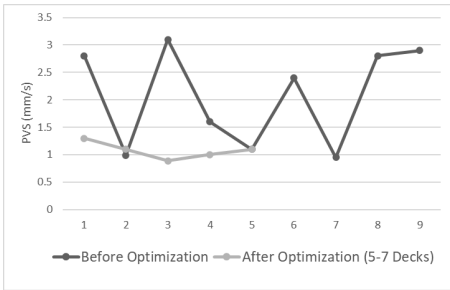

Figure 5. Vibration results non-electric vs electronic.

3.2 Blast pattern changes

The outstanding vibration results made space for significant changes in the blasting parameters. From the previous 5-7 decks per hole, the number decreased to three decks per single hole. As expected, the PPV got higher, though it was still not over the limit (Figure 6). The most important thing at that point was to keep the PPV constant, below the limit, and to avoid unpredicted peaks.

By performing the blasting optimisation on three different benches, an excellent outcome has been achieved during the trial period. Regardless of the reduction of seismic impact, the quarry production and overall blast size were increased. A comparison between 29 trial blasts with the Austin Powder E*STAR electronic initiation system and 22 blasts with non-electric detonators is shown in the table 2.

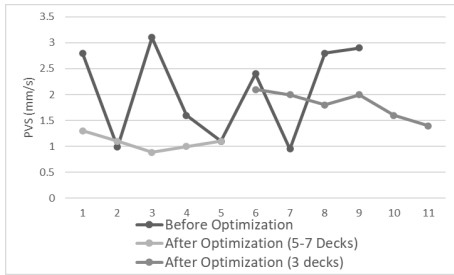

Figure 6. Vibration results including the pattern changes.

The average explosive amount per interval was increased to approximately 18.5 kg. The number of decks, delay times, and charging plan mainly depends on the blast orientation, distance to measurement points, or receiver priorities.

4 CONCLUSION

Since 2015, more than 500 blasts have been done. Blast optimisation software, with specific blast vibration analysis, was used for each of those blasts. Several measurement instruments are constantly monitoring the vibrations which are kept below the maximum limit of 3 mm/s. Nowadays, the delay range between the decks in the single hole is between 6 – 20 ms, while hole to hole delay is 12-35 ms, depending on the specific field conditions. The reduced vibrations resulted in increased blast size from single row to multi-row, where inter-row delay varies from 65 to 120 ms. The average blast size has increased by 300% since the start of the project.

Depending on the specific direction of propagation (longitudinal, transferal, or vertical) and the certain seismograph location, the K factor range is from 200 to 600 while the ‘n’ coefficient is 1.5. Due to the fact that the explosive amount per interval has been almost doubled since 2015 (13.25 kg with non-electric compared to 25 kg today), it can be said that the analytical modelling and vibration predictions software were the game changers in the blasting industry.

As a consequence of using modern blasting tools, quarries are still able to keep production level and simultaneously protect the environment. One of the most important facts, during the entire operation, was the exceptionally user-friendly

Table 2. Results after trial period.

	Non-electric blasts	E*STAR
Number of blasts	22	29
Benches	300, 320, 338	300, 320, 338
Average exp. per interval	13.25 kg	18.5 kg
Distance to caves	346 m	343 m
PPV Range	1.1 – 4.1 mm/s	0.76 – 3.7 mm/s
Average PPV	2.6 mm/s	1.8 mm/s
% of blast >= 3 mm/s	50%	10%

E*STAR system and the highly skilled blasting crew which got used to it in a very short period.

The future of blasting should be built on sustainable and environmental-friendly usage of civil explosives, detonators, and blasting equipment.

Maastricht Conference Proceedings 2022, R. Holmberg et al

Impact of fragmentation on the operational conditions of loading and haulage equipment - a case study

V. Miranda, F. Leite, A. Oliveira, T. Kouvonen & B. Saraiva
O-Pitblast Lda., Porto, Portugal

T. Kouvonen[1]
FORCIT International Ltd., Hanko, Finland

ABSTRACT: The degree of fragmentation of rock using industrial explosives is one of the most relevant factors in blasting results. Even if the fragmentation curve obtained after this phase is further altered by a subsequent crushing process, the particle size after blasting has direct implications on cost, productivity and the operational conditions of loading and haulage equipment. To make production viable and correctly organise operations at the different fronts of a mine, it is necessary and essential that the loading and haulage fleet be stationed along the length of the mine, being dependent on its efficiency, hourly productivity, number of equipment, and the compatibility between them. Normally the production plans are often prepared based on deterministic modelling, when in fact they are stochastic events. Implementing this type of methodology can lead to non-optimal intuitive choices that can undermine long-term objectives. Based on this, this study was carried out in an open-pit mine where the cycle times of the loading and haulage equipment were collected through an app, in which the data was processed to evaluate its statistical behaviour and the respective fleet operational indicators. A queue theory analysis was applied to the data in order to minimise equipment idleness and find the best configuration that would maximise the mine hourly productivity.

1 INTRODUCTION

Due to the opening of the market and global competition, producing more with fewer resources, and better quality than your competitors, have become a major challenge. Creating internal conditions that ensure the survival of organisations has become the focus of total quality control. In this situation, it is essential to implement tools and methods that help in the organisations decision making.

One of these methods is the theory of queues, which emerged in the early twentieth century with the aim of maximising the results of operations and minimise the complexity existing in production scenarios.

In the search for improving the production process, the queue theory has created an opportunity to eliminate bottlenecks, in the case of this study applied to a quarry in Portugal, an adequate haulage model was reached, reducing the waiting time of trucks near the loading queue and maximising the hourly productivity of the mine.

2 BACKGROUND

2.1 Fragmentation

Bhandari (1997) defines that the main objective of fragmentation is to obtain the largest possible volume of rock at minimum cost, guaranteeing the quantity and quality of the material, so that the

Figure 1. Existing methods for secondary blasting - (A) Use of explosives; (B) Hydraulic breaker; (C) Drop ball.

profits of the subsequent operations of this process are maximised. In blasting, this fragmentation process occurs when an explosive is inserted into a borehole and detonated, creating a state of stress followed by a violent gaseous expansion that can reach the order of 10 GPa, which causes the rock to be fragmented and displaced.

A poorly sized blasting operation may result in the generation of fine materials and/or also the generation of boulders, which may require costly secondary blasting operations, such as the use of explosives, hydraulic breakers or drop balls, significantly increasing the overall cost of the blasting operation.

Floyd (2000) elucidates that optimal blasting can be achieved if adequate fragmentation results from it, in order to achieve the lowest overall cost by combining the stages of drilling, blasting, loading, haulage, and mineral processing.

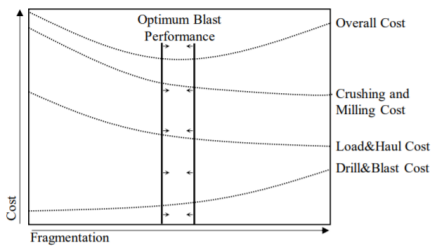

Figure 2. Mining cost relation (adapted from Efficient Blasting Techniques, (Floyd 2000).

Authors, like Shim *et al.* (2009) explain that the blasting stage is one of the most important in the entire chain, because even if the fragmentation curve obtained after this process is altered by comminution in the treatment plant, the particle size after the blasting process will have direct implications on the productivity cost and efficiency of the processes following this stage. Cunningham (2005) also mentions that if this fragmentation is not predicted and controlled, it can make a mining project unfeasible.

2.2 Effects of blasting on loading and haulage

Drilling and blasting is the process used within the mining cycle to fragment rock for excavation. Cornelius (2017) states that through efficient blasting it is possible to create excellent digging rates by providing high production cycles between the loading and haulage equipments. The term 'Diggability' refers to the measure of ease of excavation under specific operating conditions (Hall & Khorzoughi 2016).

The size of the particles generated by the blast is directly related to the time it takes for the loader to fill the bucket (Giles 2016). The bucket fill factor can be calculated as follows:

$$BF_f = \frac{V_{M.L}}{V_N} * 100 \quad (1)$$

Where BF_f = Bucket fill factor; $V_{M.L}$= Volume of material loaded in bucket (m^3); V_N= Nominal volume of bucket (m^3).

Table 1. Diggability classification based on fill factor (Hall & Khorzoughi 2016).

Material Diggability	Bucket Fill Factor
Easily Digging	95 to 105%
Medium Digging	90 to 100%
Hard Digging	85 to 95%
Very Hard Digging	80 to 90%

In a qualitative way, the bucket fill factor can be interpreted according to table 1:

The productivity of the loading equipment is directly affected by the uniformity index (Brunton, Thornton, Hodson, & Sprott 2003). If the particles that make up the muckpile present a high

uniformity index, it means that the particles are all similar, i.e., they have a very narrow granulometry, which greatly affects the filling efficiency of the bucket as more voids are created during loading. This can lead to lower productivity as each loading cycle decreases the tonnage loaded. Therefore, for better loading, it is advisable that the material being loaded has a relatively large particle size range with a low degree of uniformity. This reduces the voids in the bucket and increases the amount of material loaded in each cycle. This effect can be seen in Figure 3 based on the studies of Singh & Narendrula (2007):

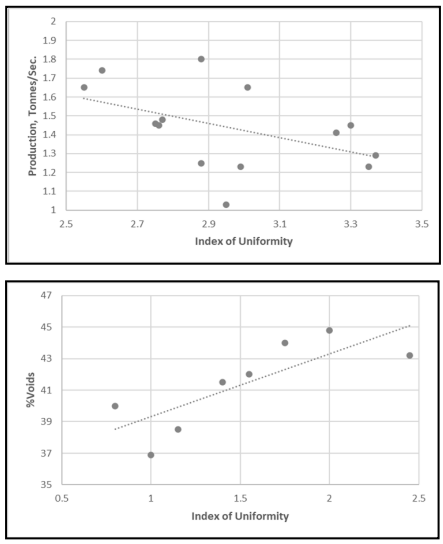

Figure 3. %Voids (first) and production rate (second) in relation to the uniformity index (Singh & Narendrula 2007), adapted.

In Figure 4, it is visible how particles fit better into the loader bucket when there are regions of granulometry (low uniformity index) that are different from more homogeneous granulometry (high uniformity index). Some studies have shown that reducing the uniformity index from 1.5 to 0.5 increases the fill factor by 15% (Cottee 2001).

It is worth pointing out that there is a certain limit to which the uniformity index can be reduced, otherwise it may make the loading and haulage operation impractical.

Haulage is designed to transport multiple bucket loads of rock. Therefore, this equipment is better suited for oversized material than the loader itself. However, if the rock blasting is done poorly and creates large boulders, it can cause problems for the haulage equipment.

Owolabi (2019) states that in addition to ensuring that a mine's production requirements are met and production costs are minimised, one of the biggest challenges for mine designers is making the right fleet choices. Figure 5 shows the range of recommended pass numbers for filling a given compatible truck:

The authors Silva (2009) and Jimeno *et al.* (2014) agree if the haulage units are well dimensioned, the loading of these cyclic machines should be done with a number of buckets that is between 3 and 5. In this way queues and idling can be avoided. The expression below shows how to obtain this result:

$$N_b = \frac{Truck\ bucket\ volume\left(m^3\right)}{Excavator\ bucket\ volume\ \left(m^3\right)} \quad (2)$$

Where N_b = Number of buckets (passes).

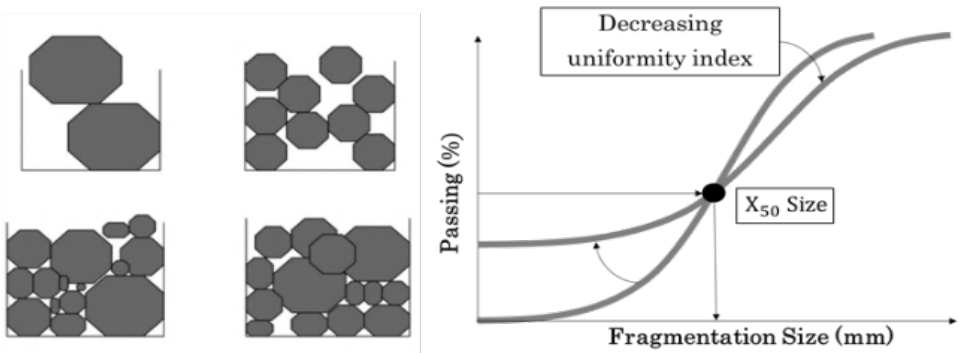

Figure 4. Effect of 'n' in fill factor (Cottee 2001), adapted.

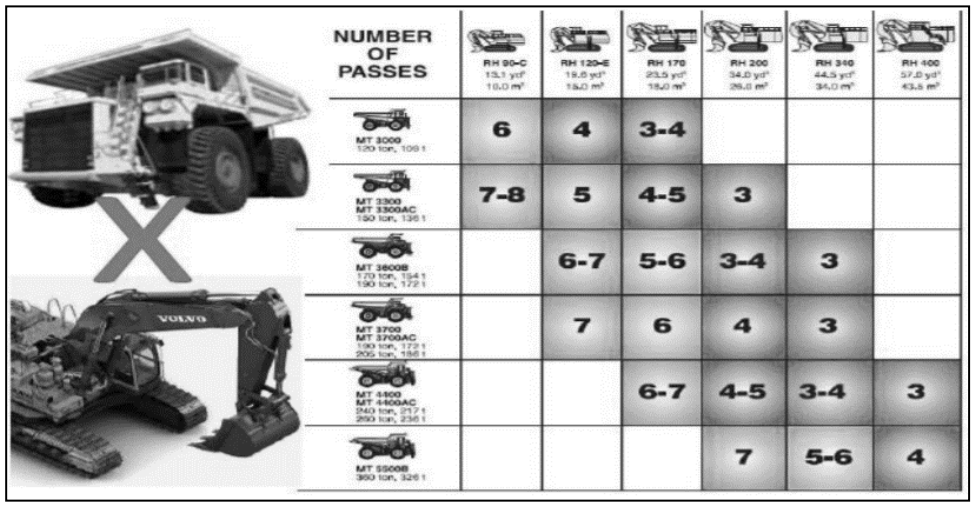

Figure 5. Number of passes from the loading equipment to the truck, (Peroni 2015).

2.3 Queueing theory

Queue Theory is an analytical method, developed by Agner, Krarup & Erlang (1909), which studies the formation of queues and their characteristics through mathematical formulas. Queues occur in the production process, whether in the form of material waiting to enter a machine to be processed, whether trucks waiting for the availability of a wheel loader to carry out the loading of a truck. Queues will happen whenever the demand exceeds the capacity to supply of the service. However, Moreira (2010) argues that queue formation is not always associated with service capacity, but also the variability in the interval between the arrival and the service time. Queue theory aims to provide data that helps in modelling a system to find an ideal balance between the costs of performing a particular service and the costs of delays caused by queues. For Prado (1999, p.33) studying the behaviour of queues is a way to modify systems in which bottlenecks exist.

2.3.1 Queuing system in mining

In mining operations, queuing systems normally originate from haulage process when trucks arrive at the loading position, crushing area or dumping sites and wait for their turns in line. In these queuing systems, trucks play a role as the customers of the system and the servers here are the loaders or crushers. A basic mining queuing system included trucks and loader can be illustrated as in Figure 6:

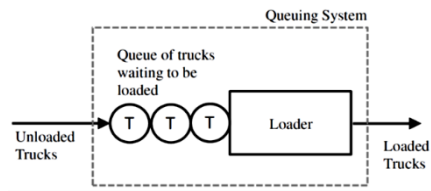

Figure 6. Truck and loader queuing system (Meredith 2012).

In cyclic queuing system, the haul route of a truck can be divided into four parts: being loaded at the loader position, loaded travelling route, unloading at the crusher and unloaded travelling route. These four stages are repeated in sequence as shown in the Figure 7:

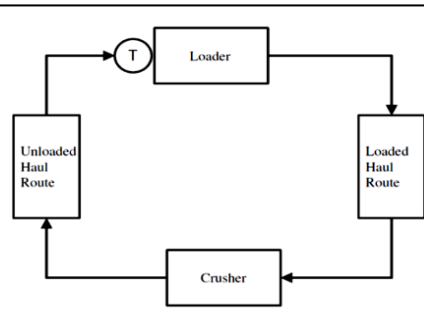

Figure 7. Cyclic queuing system (Meredith 2012).

In some mining operations, there are multiple loaders working at the same time, the cyclic

queuing system for these operations can be adjusted as a system with multiple loaders. The queuing system here is a typical of a queuing system with multiple servers, Figure 8:

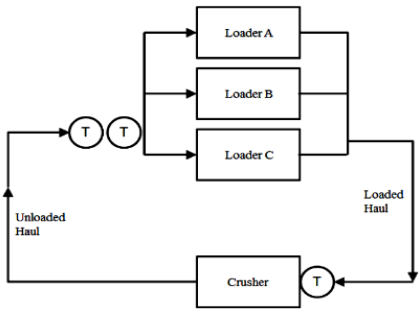

Figure 8. Cyclic queuing system with parallel loaders (Meredith 2012)

2.3.2 Description of the Gouvães da Serra quarry

The quarry in this study is located in Portugal and belongs to the Domingos da Silva Teixeira Group (DST Group) working on behalf of the Spanish energy company Iberdrola Generación. The purpose of this enterprise is to supply aggregates specifically for the construction of the Tâmega Generating System (SET), one of the largest hydroelectric projects in Europe.

The information about the loading and haulage equipment operating at the quarry is in Table 2.

2.3.3 Notation

Queueing processes are often referred to using a set of short notations in the form of (a/b/c) where each variable represents a characteristic of the system as listed in the Table 3.

Symbols 'a' and 'b' represent both types of distributions and may contain codes representing either of the common distributions. Symbol 'c' is a value and is represented with an appropriate number (when greater than 1 'S' is used) or ∞ is generally used if there is no limit on the size of the system or population source.

Table 2. Description of the loading and hauling machines and their respective capacities.

EQUIPMENT	MODEL	Nº	CAPACITY
EXCAVATOR	Komatsu PC 360	1	2.66 m3
	Komatsu PC 490	1	2.5 m3
TRUCK	Volvo A30C	1	27 ton.
	Volvo A30D	1	28 ton.
	Volvo A35D	1	32.5 ton.
	Volvo A35E	1	33.5 ton.

Table 3. Queuing notation abbreviations (Meredith, Augusta & May 2012), adapted.

Symbol	Explanation
a	Arrival distribution
b	Service distribution
c	Number of parallel serves

Table 4. Distribution abbreviations (Meredith, Augusta & May 2012).

Symbol	Explanation
M	Exponential (Markovian) or Poisson arrival process
D	Deterministic: constant distribution
E_l	Erlang distribution with parameter *l*
G	General Distribution

Figure 9. Overview of quarry Gouvães da Serra.

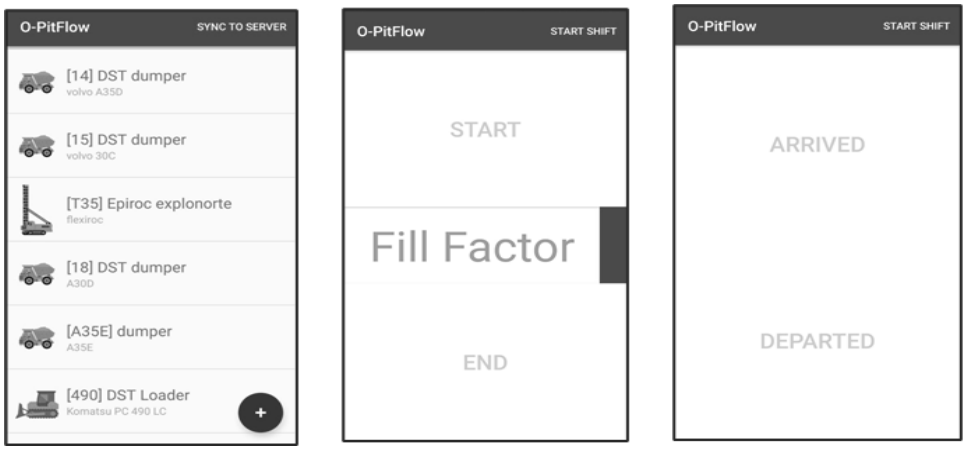

Figure 10. Screens of app used to collect date.

The loading and transport machines in this study both show a Poisson distribution for the recorded random variables of the diggability time and cycle time, as will be shown later in the article. Knowing that we have two loading machines (see Table 2) to serve the trucks, then the notation that describes the system is M/M/S.

3 DEVELOPMENT

3.1 Field Procedure

To understand what would be the ideal excavation and haulage fleet that would minimise idleness and generate good productivity for a given muckpile generated by a blasting, the O-Pitflow – a smartphone application developed by O-Pitblast – was used to collect data from the actual fleet. The version used, was made to record the arrival and departure times of the trucks for loading, as well as the diggability time of the excavators. As shown in Figure 10, the application allowed the input of the fill factor which was stipulated by the operator, with photos of the bucket whenever possible. Under these circumstances a statistical analysis was carried out divided into the following parts: Observed data and statistical behaviour to loading/haulage; medium fragmentation size (x50) vs. loading time; truck cycle time; and choice the best configuration of loading/haulage equipment.

3.2 Statistical Analysis

Observed data and statistical behaviour to loading/haulage.

The statistical study was performed to understand the behaviour of the sample data. The outliers were removed to ensure non-dispersion and to reach a 95% confidence level of the validated data. These data, when organized, showed a behaviour that approximates the probabilistic models, where state that the data from the experiments describe a Poisson distribution. Through this distribution, and based on different blasting, it was finally possible to describe the loading and haulage activity with more reliable approximations, which facilitated the understanding of each cycle phenomenon as a probability distribution.

Therefore, it can be recognised that they occur in a certain interval of time.

Through Table 5 it is possible to verify the amount of sample data collected from loading cycle of both excavator (Komatsu PC 360 NLC & Komatsu PC 490 NLC). After performing statistical tests and removing outliers it was found that the diggability time of Komatsu PC 360 NLC ranges from 2 to 40 seconds, and Komatsu PC 490 NLC ranges from 7 to 29 seconds per cycle. The figures 11 and 12 confirm through the frequency distribution, the loading time behave for both excavators. The first excavator showed validated data with standard deviation of 5.4 and a mean of 19.1 seconds per cycle (λ =17.5 seconds per cycle) and second a standard deviation of 3.9 and mean of 17 seconds per cycle (λ =16.5 seconds per cycle).

Table 5. Excavator: information about total sample collected.

Exacavator	Collected data	Statiscally validated data
Komatsu PC 360 NLC	2031	1950
Komatsu PC 490 NLC	4253	4002

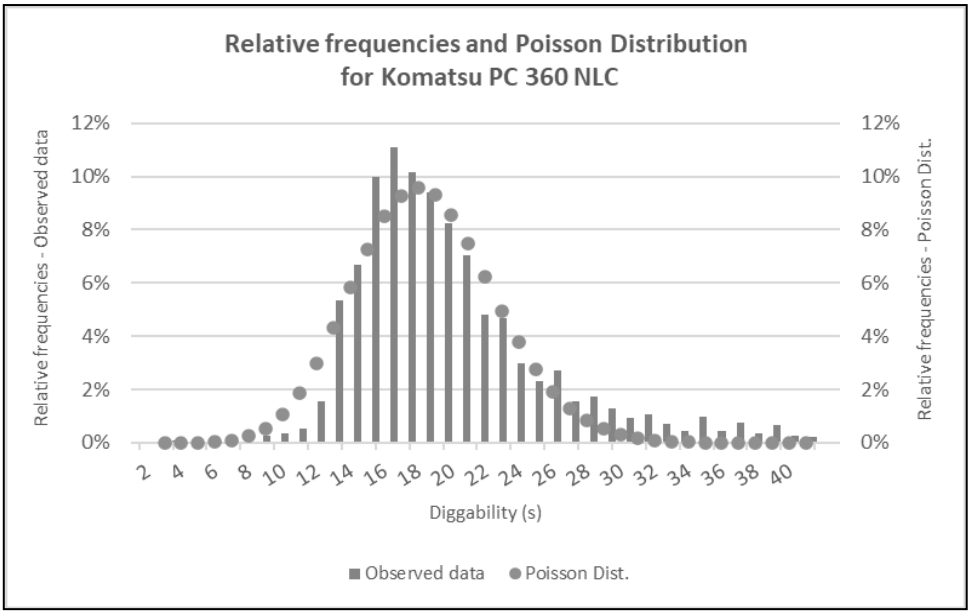

Figure 11. Relative frequencies and Poisson distribution for Komatsu PC 360 NLC.

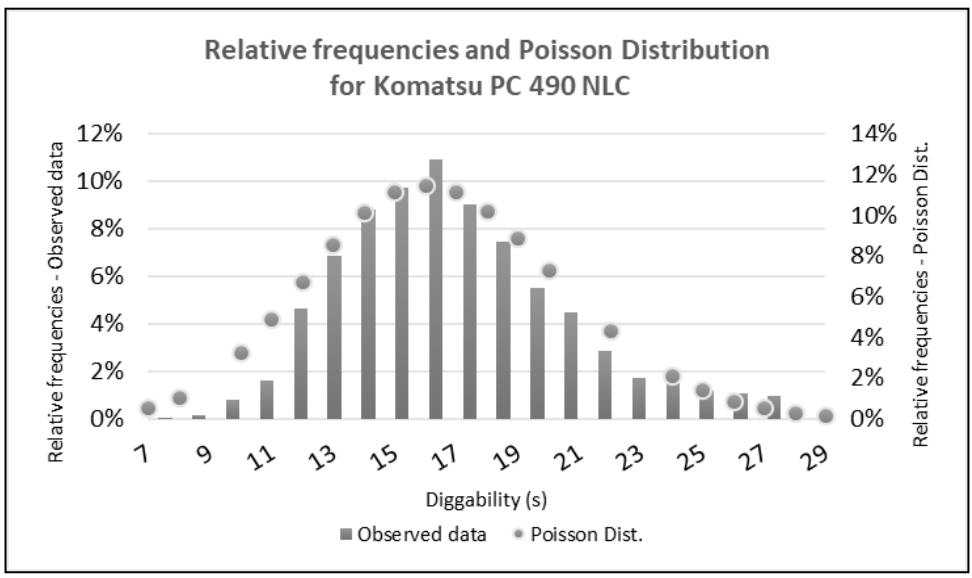

Figure 12. Relative frequencies and Poisson distribution for Komatsu PC 490 NLC.

Table 6. Truck information about total sample collected.

Truck	Collected data	Statiscally validated data
Volvo A30C	322	304
Volvo A30D	26	25
Volvo A35D	247	230
Volvo A35E	196	187

Table 6 shows the amount of collected data as well as validated data related to the cycle time of trucks equipment.

Figures 13 to 16 shows the relative frequencies of trucks cycle time (Volvo A30C, Volvo A30D, Volvo A35D and Volvo A35E respectively).

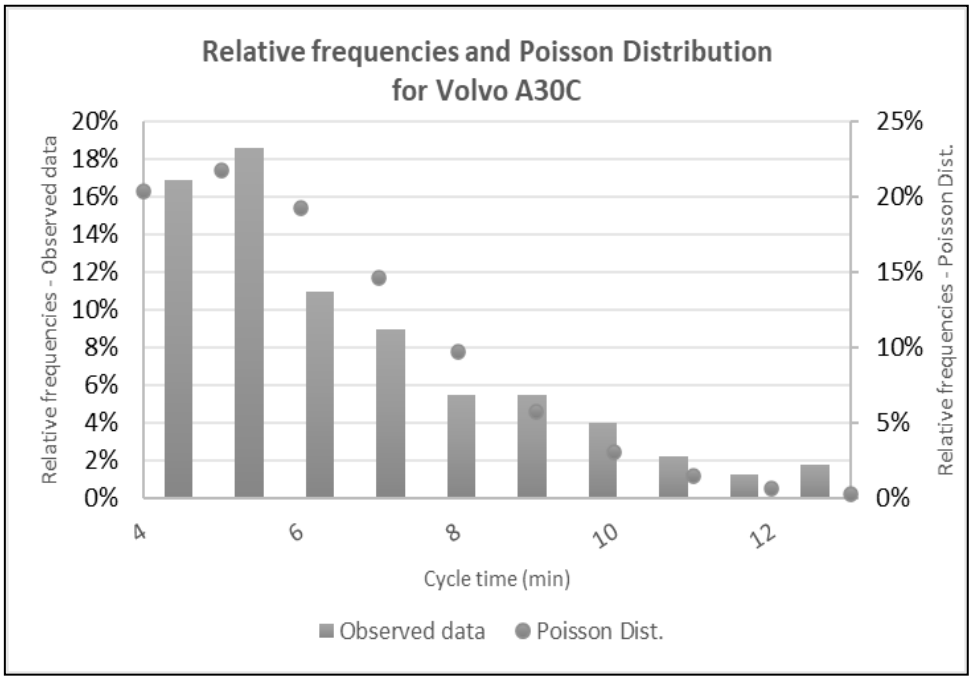

Figure 13. Relative frequencies and Poisson distribution for Volvo A30C.

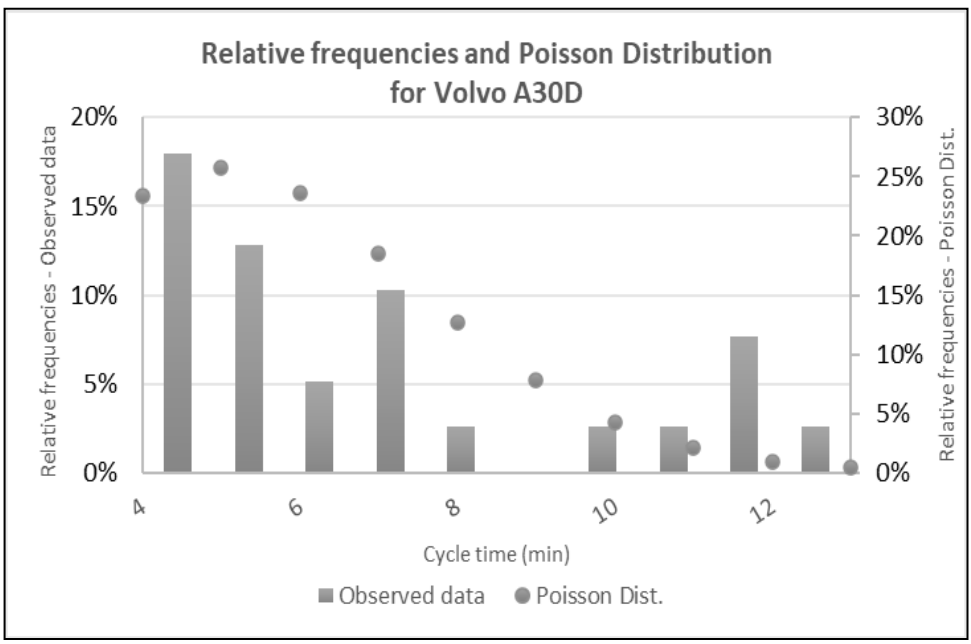

Figure 14. Relative frequencies and Poisson distribution for Volvo A30D.

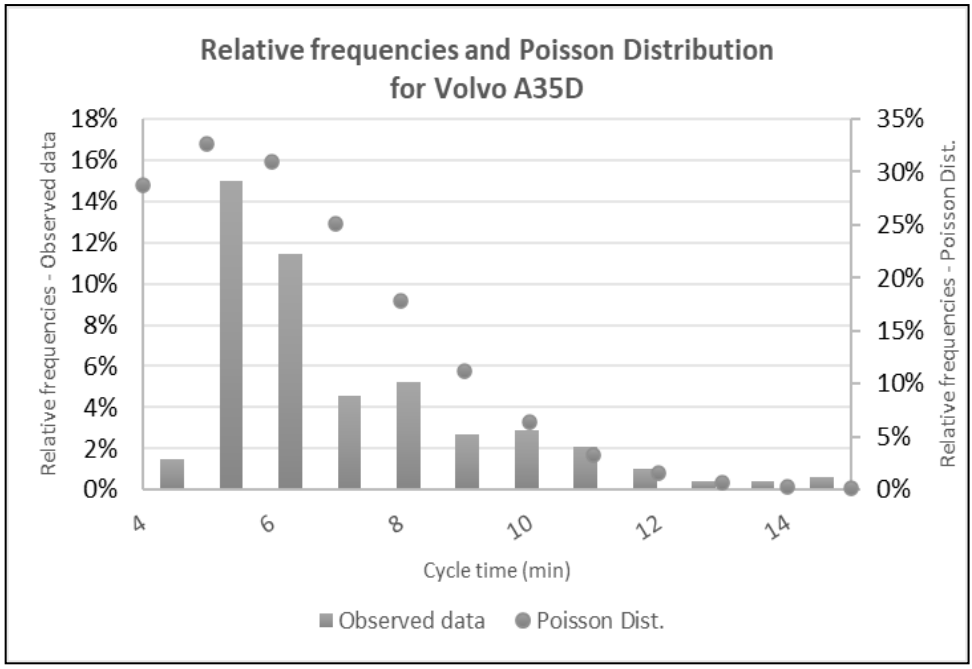

Figure 15. Relative frequencies and Poisson distribution for Volvo A35D.

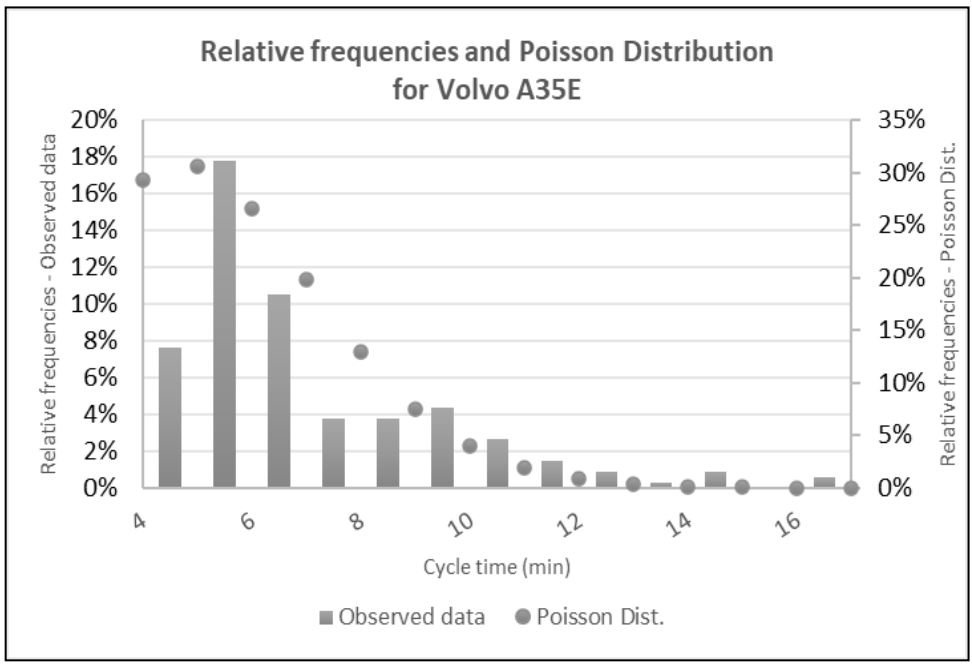

Figure 16. Relative frequencies and Poisson distribution for Volvo A35E.

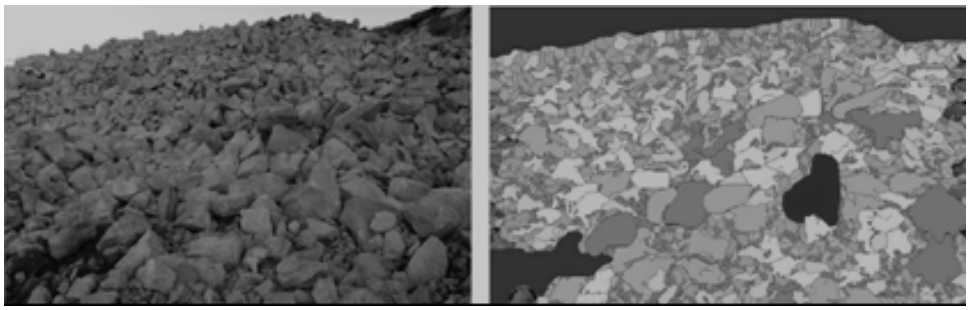

Figure 17. Particle size analysis of one of the muckpiles in this study.

Due to the high variability of the trucks cycle time, a visual inspection was carried out to remove the outliers. When analysing the model behaviour, it was also confirmed that the data follows a Poisson distribution. Through this analyse the following conclusions could be made:

- Volvo A30C: cycle time ranging from 4 to 13 minutes per cycle (λ = 5.32 minutes per cycle);
- Volvo A30D: cycle time ranging from 4 to 13 minutes per cycle (λ = 5.50 minutes per cycle);
- Volvo A35E: cycle time ranging from 4 to 15 minutes per cycle (λ = 5.68 minutes per cycle);
- Volvo A35E: cycle time ranging from 4 to 16 minutes per cycle (λ = 5.22 minutes per cycle);

3.3 Mean particle size & loading time

After the particle size analysis using the WipFrag software, it was possible to observe that there is a relationship between the loading time and the average fragment size (X50).

Following this, an algorithm was developed to simulate the interaction between these two variables. Once this information was available, the objective of the study was to anticipate and predict loading and haulage times for a given muckpile.

Generated modelling was used to analyse a linear regression between mean particle size and loading time. Although the data is not statistically significant by Fisher's F-test, the literature shows a strong linear association between these two variables, as cited by Giles (2016).

On the basis of *X*50 it was possible to estimate the average loading time, but not precisely. Assuming that the linear regression had normally distributed residuals around the point found on the line, we were able to determine the confidence interval for the constant on the line and thus determine the standard deviation of the sample. This made it possible to simulate a normally distributed number with these parameters around the regression line. This value was then used as the λ parameter to simulate the loading time of the excavators. The random relationship obtained by the confidence level allowed a more realistic approximation to the phenomenon of cycle activity of the monitored equipment. Below is represented the regression used to estimate the diggability time of the loading machines:

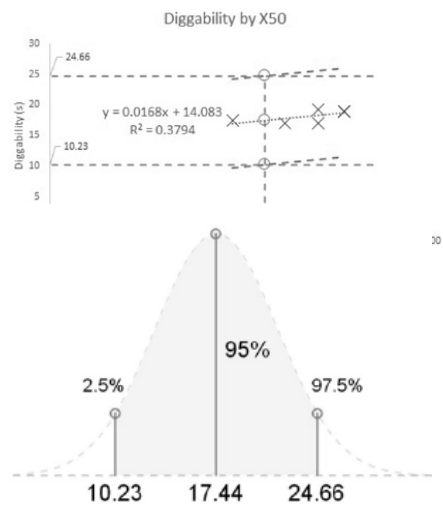

Figure 18a and 18b. Diagram representing the approximation of a straight line with upper and lower limitations conferred by a confidence interval for the normal distribution of diggability.

The application of the method described, made it possible to calculate the random time as many times as necessary for different $X50$. The data presented in Figure 18 was based on 6 blasts using the equipment listed in Table 2.

3.4 Truck cycle time

For the simulation process of the truck cycle time, a simple procedure was elaborated. Once the λ of the Poisson distribution and the standard deviation were known after the outlier removal process, a random number was generated to determine what would be the total cycle time of the truck. This process was done for all the haulage machines.

3.5 Simulation

Initially it was established that the blast design, the products applied and the characteristics of the geology would be constant, i.e. the same situation for all cases. Currently the quarry works as follows:

- Type of explosive: Emulsion
- Type of ignition system: Non-electric
- Burden, spacing, stemming, subdrilling and bench height: 2.8 m, 3.7 m, 1.9 m, 0.9 m and 10 m
- Drill hole diameter: 76.2 mm
- Type of drill rig: Top hammer drilling
- Powder factor: 0.41 kg/m^3
- Volume of rock per blast: 18.000 m^3
- Rock factor: 14.3

Next, the combinations of equipment to be evaluated were defined, as shown in Table 7:

Based on the current operational model of the

Table 7. Combinations defined for the simulations of the loading and haulage operation.

#Simulation	Nº of excavators	Nº of trucks	Description
1	2	4	Two excavators with 2.66 and 3.5 m³ buckets and four trucks with 30 tons.
2	1	4	A single excavator with a 2.66 m³ bucket and four trucks with a capacity of 30 tons.
3	1	4	A single excavator with a 3.5 m³ bucket and four trucks with a capacity of 30 tons.
4	2	4	Two excavators with 3.5 m³ buckets and four trucks with 30 tons.
5	2	3	Two excavators with 2.66 and 3.5 m³ buckets and three trucks with 30 tons.
6	2	3	Two excavators with 3.5 m³ buckets and three trucks with 30 tons.
7	1	3	A single excavator with a 3.5 m³ bucket and three trucks with a capacity of 30 tons.
8	1	3	A single excavator with a 2.66 m³ bucket and three trucks with a capacity of 30 tons.
9	1	2	A single excavator with a 2.66 m³ bucket and two trucks with a capacity of 30 tons.
10	1	2	A single excavator with a 3.5 m³ bucket and two trucks with a capacity of 30 tons.
11	2	2	Two excavators with 3.5 m³ buckets and two trucks with 30 tons.
12	2	2	Two excavators with 2.65 and 3.5 m³ buckets and two trucks with 30 tons.
13	2*	4	Two excavators with 3.5 and 4.5* m³ buckets and four trucks with 30 tons.
14	2*	3	Two excavators with 3.5 and 4.5* m³ buckets and three trucks with 30 tons.
15	2	5**	Two excavators with 3.5 and 4.5* m³ buckets and five trucks with 30 tons.

** Larger bucket capacity for simulation effects.*
***Extra truck in operation.*

quarry, described previously, we sought to find arrangements that would lead to a reduction in related costs, as well as the best performance for the same annual production. For simulation purposes, we defined that the trucks (Volvo A30C, A30D, A35D and A35E) would have the same capacity of 30 tons and for the excavators the two existing ones (Komatsu PC 360 NLC and PC 490 NLC) and one 'supposed' to have a 4.5 m³ bucket were used.

3.6 Results

Table 8 shows the summary of the outcome of the simulations indicated previously, assuming an annual production of 500,000 m³ with shift costs equivalent to 1.000€. In the Tables found in Appendix A, the information and results of each proposed combination are presented in detail. In Table 8, under the current conditions (two loading machines and trucks), the best alternative would be the 7th, with savings of 13,474.48€/year. But when we take into account the work time spent (10.38 hours more) it would not be interesting, as it could disturb the quarry operations.

If we add the possibility of changes in the capacity of the equipment, preliminarily, a simple change of the bucket of the Komatsu PC360, if possible, from 2.66 m³ to 3.5 m³, would lead to a reduction in the estimated cost by 38.340€/year in the expedient (21.89 versus 23.86 hours), as explained in the 4th arrangement.

If we increase the bucket capacity to 4.5 m³, we can arrive at scenarios 13 and 14, where it is notable that a larger number of trucks would benefit the operation. This is confirmed by adding an extra truck (scenario 15), totalling five, where we would reach a situation where the cost per cubic metre of rock would be 2.80€ (0.17€ less than the current one, resulting in 82,062€/year), in addition to enabling greater blasting, since it would take 17.38 hours to complete the removal of the material, making it the best simulation of all if this scenario is possible.

4 CONCLUSIONS

With the help of the O-PitFlow application, it was possible to collect more detailed information about the excavation capacity, muckpile loading cycle and the trucks.

Statistical treatment for both the excavation and transport cycle time data revealed a good correlation between the time-class distribution of these parameters and the Poisson distribution.

Data collection allowed the application of simulation strategies that included various scenarios to obtain the most viable option for the drilling, blasting, loading, and hauling phases. This type of analysis is of utmost importance to engineers and technicians who, in their daily work, try to make estimates based on these types of operations, and allows them to create a plan taking into account operational variability. In this study it was seen that it is possible to achieve very significant annual savings of more than 80,000€.

For the simulation results presented throughout this paper we have not taken into consideration the extra investment (acquisition), fuel and maintenance costs for a new truck or for increasing the capacity of an excavator.

Table 8. General summary of the results obtained in the simulation of the equipment combinations.

#	Time to remove the muckpile	Nº of shifts	Shift cost	Truck costs	Loading cost	Blasting cost	Total cost of operations	Total cost of operations + shifts	Cost per cubic meter of rock	Estimated annual cost
1	23.86h	2.98	2 982.64 €	9 571.00 €	5 968.00 €	40 807.68 €	56 346.68 €	59 329.32 €	2.97€/m3	1 483 233.09 €
2	39.46h	4.93	4 932.92 €	15 782.00 €	3 946.00 €	40 807.68 €	60 535.68 €	65 468.60 €	3.27€/m3	1 636 715.03 €
3	30.07h	3.76	3 758.16 €	12 043.00 €	3 007.00 €	40 807.68 €	55 857.68 €	59 615.84 €	2.98€/m3	1 490 396.11 €
4	21.89h	2.74	2 736.04 €	8 775.00 €	5 477.00 €	40 807.68 €	55 059.68 €	57 795.73 €	2.89€/m3	1 444 893.16 €
5	30.69h	3.84	3 835.66 €	9 237.00 €	7 680.00 €	40 807.68 €	57 724.68 €	61 560.34 €	3.08€/m3	1 539 008.61 €
6	28.60h	3.57	3 574.69 €	8 595.00 €	7 150.00 €	40 807.68 €	56 552.68 €	60 127.37 €	3.01€/m3	1 503 184.30 €
7	34.25h	4.28	4 280.66 €	10 277.00 €	3 425.00 €	40 807.68 €	54 509.68 €	58 790.34 €	2.94€/m3	1 469 758.61 €
8	40.79h	5.10	5 098.26 €	12 245.00 €	4 079.00 €	40 807.68 €	57 131.68 €	62 229.95 €	3.11€/m3	1 555 748.71 €
9	53.37h	6.67	6 671.08 €	10 685.00 €	5 337.00 €	40 807.68 €	56 829.68 €	63 500.76 €	3.18€/m3	1 587 519.02 €
10	47.24h	5.91	5 905.42 €	9 458.00 €	4 724.00 €	40 807.68 €	54 989.68 €	60 895.10 €	3.04€/m3	1 522 377.53 €
11	43.05h	5.38	5 381.63 €	8 633.00 €	10 773.00 €	40 807.68 €	60 213.68 €	65 595.32 €	3.28€/m3	1 639 882.91 €
12	43.26h	5.41	5 407.43 €	8 661.00 €	10 818.00 €	40 807.68 €	60 286.68 €	65 694.12 €	3.28€/m3	1 642 352.88 €
13	21.05h	2.63	2 631.25 €	8 458.00 €	5 265.00 €	40 807.68 €	54 530.68 €	57 161.93 €	2.86€/m3	1 429 048.37 €
14	27.15h	3.39	3 394.20 €	8 184.00 €	6 798.00 €	40 807.68 €	55 789.68 €	59 183.89 €	2.96€/m3	1 479 597.15 €
15	17.38h	2.17	2 172.15 €	8 722.00 €	4 345.00 €	40 807.68 €	53 874.68 €	56 046.84 €	2.80€/m3	1 401 170.93 €

REFERENCES

Bhandari, Sushil. 1997. Engineering rock blasting operations. *Rotterdam Brookfield: A.A.Balkema*.

Brunton, I., D. Thornton, D. Hodson, & D. Sprott. 2003. Impact of blast fragmentation on hydraulic excavator dig time. *Fifth Large Open Pit Mining Conference* 10.

Camelo, G., Coelho, A., Borges, A. & Souza, R. 2010. Teoria das filas e da simulacao applicada ao embarque de minerio de ferro e manganes no terminal Maritimo de Ponta da Madeira. *XXX Encontro Nacional de Engenharia de Producao* 14.

Cornelius, M. 2017. Mine production improvement through haulage optimisation. *Queensland: The University of Queensland.*

Cottee, S. 2001. Impact of fragmentation on truck and loader productivity. *The University of Queensland*.

Cunningham, C. 2005. The Kuz-Ram fragmentation model – 20 years on. *European Federation of Explosives Engineers*.

Floyd, J. 2000. Efficient blasting techniques. *Blast Dynamics*.

Giles, E. 2016. Improving quarry production rates by reducing bucket fill time. *International Society of Explosives Engineers.*

Hall, R. & Khorzoughi, M.B. 2016. Diggability assessment in open pit mines: a review. *Mining and Mineral Engineering*.

Jimeno, C., Jimeno, E.,. Bérmudez, P. & Degea, A. 2014. Manual de transporte con voloquetes y diseño de pistas mineras. Madrid: *Gráficas Arias Montano, S. A.*

May, M. 2012. Applications of Queuing Theory for open-pit truck/shovel haulage systems.

Moreira, D. A. 2010. Pesquisa Operacional: Curso Introdutório. *São Paulo: Cengage Learning*.

Owolabi, A. 2019. Loading and haulage equipment selection for optimum production in a granite quarry. *International Journal of Mining Science* (IJMS) 6.

Peroni, R. L. 2015. Introdução da lavra à céu aberto. *Rio Grande do Sul: Universidade Federal do Rio Grande do Sul.*

Prado, D. S. 1999. Teoria das Filas e da Simulação. Belo Horizonte: *Editora de Desenvolvimento Gerencial.*

Shim, H. J., Ryu, D. W., Chung, S. K., Synn, J. H. & Song, J.J.. 2009. Optimised blasting design for large-scale quarrying based on a 3-D spatial distribution of rock factor. *International Journal of Rock Mechanics and Mining Sciences.*

Silva, V. C. 2009. Apostila de Carregamento e transporte de rochas. *Ouro Preto: Escola de Minas da Universidade de Ouro Preto*.

Singh, S. & Narendrula, R. 2007. Factors affecting the productivity of loaders in surface mines. *International Journal of Mining, Reclamation and Environment*, 14.

APPENDIX

Data from the proposed combinations for simulation are provided on the following pages.

1. Times and costs resulting from the simulation of the combination 1.

Combination 1	Excavator		Truck			
	2.66 m^3	3.5 m^3	A30D	A30C	A30E	A35D
Loading (s)	71106 (82.78%)	39205 (45.61%)	28729 (33.87%)	27447 (31.87%)	26316 (30.55%)	27819 (32.18%)
Idle (s)	14794 (17.22%)	46756 (54.39%)	-	-	-	-
In queue (s)	-	-	2403 (2.80%)	4262 (4.95%)	3005 (3.49%)	4201 (4.86%)
Travelling (s)	-	-	54720 (63.74%)	54420 (63.18%)	56820 (65.96%)	54420 (62.96%)
Average in queue (s)	44	140	14	25	18	26
Average load completion (s)	214	117	169	163	157	173
Average delivery of material (s)	-	-	322	324	338	338
Total cost (€)	2,386.00 €	3,582.00 €	2,385.00 €	2,392.00 €	2,393.00 €	2,401.00 €

Final Result			
Excavators cost	Trucks cost	Blasting cost	Total
5,968.00 €	9,571.00 €	40,807.68 €	56,346.68 €

2. Times and costs resulting from the simulation of the combination 2.

Combination 2	Excavator	Truck			
	2.66 m^3	A30C	A35D	A30D	A35E
Loading (s)	141871 (99.86%)	35922 (25.38%)	34353 (24.18%)	36031 (25.35%)	35565 (24.97%)
Idle (s)	197 (0.14%)	-	-	-	-
In queue (s)	-	51992 (36.73%)	50337 (35.44%)	52035 (36.61%)	50643 (35.56%)
Travelling (s)	-	53640 (37.89%)	57360 (40.38%)	54060 (38.04%)	56220 (39.47%)
Average in queue (s)	0	308	311	308	303
Average load completion (s)	213	213	212	213	213
Average delivery of material (s)	-	317	354	320	337
Total cost (€)	3,946.00 €	3,932.00 €	3,946.00 €	3,948.00 €	3,956.00 €

Final Result			
Excavators cost	Trucks cost	Blasting cost	Total

3. Times and costs resulting from the simulation of the combination 3.

Combination 3	Excavator	Truck			
	3.5 m^3	A30D	A30C	A35D	A35E
Loading (s)	106657 (98.54%)	26830 (24.84%)	25705 (23.70%)	26476 (24.40%)	27646 (25.46%)
Idle (s)	1578 (1.46%)	-	-	-	-
In queue (s)	-	28061 (25.98%)	27950 (25.78%)	27440 (25.29%)	28149 (25.92%)
Travelling (s)	-	53100 (49.17%)	54780 (50.52%)	54600 (50.31%)	52800 (48.62%)
Average in queue (s)	2	167	173	166	164
Average load completion (s)	160	160	159	160	161
Average delivery of material (s)	-	316	338	331	307
Total cost (€)	3,007.00 €	3,000.00 €	3,012.00 €	3,014.00 €	3,017.00 €

Final Result

Excavators cost	Trucks cost	Blasting cost	Total

4 Times and costs resulting from the simulation of the combination 4.

Combination 4	Excavator		Truck			
	3.5 m^3	3.5 m^3	A30C	A30D	A35E	A35D
Loading (s)	53326 (67.67%)	39089 (49.54%)	23343 (29.60%)	22390 (28.37%)	24304 (30.80%)	22378 (28.25%)
Idle (s)	25472 (32.33%)	39816 (50.46%)	-	-	-	-
In queue (s)	-	-	1525 (1.93%)	2228 (2.82%)	2175 (2.75%)	2227 (2.81%)
Travelling (s)	-	-	54000 (68.47%)	54300 (68.81%)	52440 (66.45%)	54600 (68.94%)
Average in queue (s)	76	119	9	14	12	14
Average load completion (s)	160	117	137	137	139	141
Average delivery of material (s)	-	-	318	333	300	343
Total cost (€)	2,189.00	3,288.00	2,191.00	2,192.00	2,192.00	2,200.00

Final Result

Excavators cost	Trucks cost	Blasting cost	Total
5,477.00 €	8,775.00 €	40,807.68 €	55,059.68 €

5. Times and costs resulting from the simulation of the combination 5.

Combination 5	Excavator		Truck		
	2.66 m^3	3,5 m^3	A30C	A35E	A30D
Loading (s)	70892 (64,17%)	39399 (35,60%)	36937 (33,38%)	36917 (33,29%)	36437 (32,84%)
Idle (s)	39575 (35,83%)	71262 (64,38%)	-	-	-
In queue (s)	-	-	1843 (1,66%)	2404 (2,17%)	1670 (1,51%)
Travelling (s)	-	-	71880 (64,96%)	71580 (64,54%)	72840 (65,65%)
Average in queue (s)	119	213	8	11	7
Average load completion (s)	213	118	169	164	163
Average delivery of material (s)	-	-	330	318	325
Total cost (€)	3 069,00	4 611,00	3 074,00	3 081,00	3 082,00

Final Result

Excavators cost	Trucks cost	Blasting cost	Total
7 680,00 €	9 237,00 €	40 807,68 €	57 724,68 €

6. Times and costs resulting from the simulation of the combination 6.

Combination 6	Excavator		Truck		
	3.5 m^3	3.5 m^3	A30D	A35E	A30C
Loading (s)	39066 (37.95%)	52783 (51.26%)	29053 (28.19%)	31982 (31.01%)	30814 (29.86%)
Idle (s)	63885 (62.05%)	50189 (48.74%)	-	-	-
In queue (s)	-	-	943 (0.91%)	889 (0.86%)	1118 (1.08%)
Travelling (s)	-	-	73080 (70.90%)	70260 (68.13%)	71280 (69.06%)
Average in queue (s)	191	151	4	4	5
Average load completion (s)	117	159	138	139	136
Average delivery of material (s)	-	-	346	305	315
Total cost (€)	4,290.00	2,860.00	2,863.00	2,865.00	2,867.00

Final Result

Excavators cost	Trucks cost	Blasting cost	Total
7,150.00 €	8,595.00 €	40,807.68 €	56,552.68 €

7. Times and costs resulting from the simulation of the combination 7.

Combination 7	Excavator	Truck		
	3.5 m^3	A30C	A30D	A35E
Loading (s)	106397 (86.30%)	36651 (29.76%)	33883 (27.48%)	35863 (29.03%)
Idle (s)	16886 (13.70%)	-	-	-
In queue (s)	-	16173 (13.13%)	14961 (12.13%)	18000 (14.57%)
Travelling (s)	-	70320 (57.10%)	74460 (60.39%)	69660 (56.39%)
Average in queue (s)	25	71	70	80
Average load completion (s)	160	161	158	159
Average delivery of material (s)	-	308	348	310
Total cost (€)	3,425.00	3,421.00	3,425.00	3,431.00

Final Result

Excavators cost	Trucks cost	Blasting cost	Total
3,425.00 €	10,277.00 €	40,807.68 €	54,509.68 €

8. Times and costs resulting from the simulation of the combination 8.

Combination 8	Excavator	Truck		
	2.66 m^3	A35E	A30C	A30D
Loading (s)	141502 (96.37%)	46917 (31.96%)	47903 (32.63%)	46682 (31.70%)
Idle (s)	5328 (3.63%)	-	-	-
In queue (s)	-	29846 (20.33%)	30150 (20.54%)	29528 (20.05%)
Travelling (s)	-	70020 (47.70%)	68760 (46.83%)	71040 (48.24%)
Average in queue (s)	8	136	133	134
Average load completion (s)	212	213	211	212
Average delivery of material (s)	-	318	303	323
Total cost (€)	4,079.00	4,077.00	4,078.00	4,090.00

Final Result

Excavators cost	Trucks cost	Blasting cost	Total
4,079.00 €	12,245.00 €	40,807.68 €	57,131.68 €

9. Times and costs resulting from the simulation of the combination 9.

Combination 9	Excavator	Truck	
	2.66 m^3	A30D	A35E
Loading (s)	142105 (73.96%)	69633 (36.24%)	72472 (37.65%)
Idle (s)	50022 (26.04%)	-	-
In queue (s)	-	12189 (6.34%)	12615 (6.55%)
Travelling (s)	-	110340 (57.42%)	107400 (55.80%)
Average in queue (s)	75	37	37
Average load completion (s)	213	214	213
Average delivery of material (s)	-	338	315
Total cost (€)	5,337.00	5,338.00	5,347.00

Final Result			
Excavators cost	Trucks cost	Blasting cost	Total
5,337.00 €	10,685.00 €	40,807.68 €	56,829.68 €

10. Times and costs resulting from the simulation of the combination 10.

Combination 10	Excavator	Truck	
	3.5 m^3	A35E	A30D
Loading (s)	106593 (62.67%)	54595 (32.09%)	51998 (30.53%)
Idle (s)	63483 (37.33%)	-	-
In queue (s)	-	7324 (4.30%)	8038 (4.72%)
Travelling (s)	-	108240 (63.61%)	110280 (64.75%)
Average in queue (s)	95	22	25
Average load completion (s)	160	161	159
Average delivery of material (s)	-	318	337
Total cost (€)	4,724.00	4,727.00	4,731.00

Final Result			
Excavators cost	Trucks cost	Blasting cost	Total
4,724.00 €	9,458.00 €	40,807.68 €	54,989.68 €

11. Times and costs resulting from the simulation of the combination 11.

Combination 11	Excavator		Truck	
	3.5 m^3	3.5 m^3	A30D	A35E
Loading (s)	52971 (34.18%)	39141 (25.21%)	46130 (29.72%)	45982 (29.55%)
Idle (s)	102020 (65.82%)	116101 (74.79%)	-	-
In queue (s)	-	-	0	0
Travelling (s)	-	-	109080 (70.28%)	109620 (70.45%)
Average in queue (s)	306	348	0	0
Average load completion (s)	159	117	139	137
Average delivery of material (s)	-	-	329	327
Total cost (€)	4,305.00	6,468.00	4,311.00	4,322.00

Final Result

Excavators cost	Trucks cost	Blasting cost	Total
10,773.00 €	8,633.00 €	40,807.68 €	60,213.68 €

12. Times and costs resulting from the simulation of the combination 12.

Combination 12	Excavator		Truck	
	2.66 m^3	3.5 m^3	A35E	A30D
Loading (s)	51722 (33.21%)	53683 (34.45%)	53614 (34.40%)	51791 (33.21%)
Idle (s)	104012 (66.79%)	102148 (65.55%)	-	-
In queue (s)	-	-	0	0
Travelling (s)	-	-	102240 (65.60%)	104160 (66.79%)
Average in queue (s)	312	306	0	0
Average load completion (s)	155	161	158	158
Average delivery of material (s)	-	-	301	319
Total cost (€)	6,489.00	4,329.00	4,329.00	4,332.00

Final Result

Excavators cost	Trucks cost	Blasting cost	Total
10,818.00 €	8,661.00 €	40,807.68 €	60,286.68 €

13. Times and costs resulting from the simulation of the combination 13.

Combination 13	Excavator		Truck			
	3.5 m^3	4.5 m^3	A35D	A30D	A30C	A35E
Loading (s)	39059 (51.54%)	41098 (54.18%)	19462 (25.67%)	20050 (26.38%)	20627 (27.05%)	20018 (26.21%)
Idle (s)	36721 (48.46%)	34749 (45.82%)	-	-	-	-
In queue (s)	-	-	1285 (1.69%)	1302 (1.71%)	1820 (2.38%)	1342 (1.76%)
Travelling (s)	-	-	55080 (72.64%)	54660 (71.91%)	53820 (70.57%)	55020 (72.03%)
Average in queue (s)	110	104	8	8	11	8
Average load completion (s)	117	123	121	120	121	119
Average delivery of material (s)	-	-	342	327	315	328
Total cost (€)	3,158.00	2,107.00	2,106.00	2,111.00	2,119.00	2,122.00

Final Result

Excavators cost	Trucks cost	Blasting cost	Total
5,265.00 €	8,458.00 €	40,807.68 €	54,530.68 €

14. Times and costs resulting from the simulation of the combination 14.

Combination 14	Excavator		Truck		
	3.5 m^3	4.5 m^3	A30C	A35E	A30D
Loading (s)	39477 (40.29%)	41402 (42.35%)	27610 (28.18%)	28177 (28.68%)	25092 (25.50%)
Idle (s)	58507 (59.71%)	56351 (57.65%)	-	-	-
In queue (s)	-	-	1075 (1.10%)	516 (0.52%)	592 (0.60%)
Travelling (s)	-	-	69300 (70.72%)	69540 (70.79%)	72720 (73.90%)
Average in queue (s)	175	169	5	2	3
Average load completion (s)	118	124	121	121	121
Average delivery of material (s)	-	-	304	300	351
Total cost (€)	4,083.00	2,715.00	2,722.00	2,729.00	2,733.00

Final Result

Excavators cost	Trucks cost	Blasting cost	Total
6,798.00 €	8,184.00 €	40,807.68 €	55,789.68 €

15. Times and costs resulting from the simulation of the combination 15.

Combination 15	Excavator		Truck				
	3.5 m^3	4.5 m^3	A35E	A30D	A30D	A30C	A35D
Loading (s)	38971 (62.30%)	41548 (66.39%)	17089 (27.33%)	15647 (24.99%)	15973 (25.43%)	16494 (26.24%)	15316 (24.25%)
Idle (s)	23587 and (37.70%)	21031 (33.61%)	-	-	-	-	-
In queue (s)	-	-	2777 (4.44%)	1677 (2.68%)	1786 (2.84%)	1841 (2.93%)	1822 (2.88%)
Travelling (s)	-	-	42660 (68.23%)	45300 (72.33%)	45060 (71.73%)	44520 (70.83%)	46020 (72.87%)
Average in queue (s)	71	63	19	13	13	14	14
Average load completion (s)	117	124	120	120	120	123	121
Average delivery of material (s)	-	-	298	348	339	332	362
Total cost (€)	2,607.00	1,738.00	1,737.00	1,740.00	1,745.00	1,746.00	1,754.00

Final Result

Excavators cost	Trucks cost	Blasting cost	Total
4,345.00 €	8,722.00 €	40,807.68 €	53,874.68 €

Maastricht Conference Proceedings 2022, R. Holmberg et al

Modelling and determining the effective parameters in ore dilution in Sarcheshmeh copper mine

V. Kala & E. Kubat
Austin Detonator s.r.o., Vsetin, Czech Republic

G.R. Jabalbarzai
Master of Sarcheshmeh Copper Mine Ore Control

A**.** Nikkhah
Supervisor of mining projects, Tehran, Iran

G.R. Saeedi
Mining Engineering Department, Shahid Bahonar University of Kerman, Kerman, Iran

J. Hakimi
Manager of Sarcheshmeh Copper Mine

P. Tahernejad Javazm
Manager of Sarcheshmeh Copper Mining Engineering

ABSTRACT: The grade control process in mines is aimed at maximising the value of extracted ore deposits. In this research, the sources of dilution and also strategies in drilling, blasting and loading units were studied in Sarcheshmeh copper mine. The result of this study was to determine the 18 factors of dilution in five groups including geometry, uncertainty in knowledge of the *in situ* ore boundaries, blast movement, mining errors and weather conditions. Most of the blasting is controlled by bulk blasting type, but due to blast patterns and time delay sequences, the maximum dilution rate is 13.17%. The parameters, including stemming length and spacing, increase the dilution, however the hole diameter, specific drilling and ratio of length to width of blast block decreases the dilution. In order to control dilution, strategies such as switching blast types, post blasting geological control and loading fleet dispatching will be effective.
Keywords: blasting, ore dilution, specific drilling, SPSS software, Sarcheshmeh copper mine.

1 INTRODUCTION

Dilution in mines, such as underground and open pits, disrupts the process of mineral operations, and increases all mining costs from extraction to product sales progressively (Little 2015, Smith *et al.* 2015, Domingo *et al.* 2015, Wang *et al.* 2011, Najafi *et al.* 2014). Dilution is one of the mining problems that, in addition to economically imposing more mining costs, puts a lasting

negative impact on the lives of humans and creatures of later generations. The degradation and environmental pollutants resulting from the dilution of mining are considered to be a life-threatening factor. In order to prevent the negative effects, the dilution of a means is not limited to identifying and preventing it in the mining industry (Little 2015).

Mining dilution is one of the most important factors affecting the economy of mining projects. While all efforts are made to identify and calculate all the cost items of a project, ignoring the phenomenon of dilution or lack of accurate calculation of this quantity results in incomplete economic estimates. This is usually due to lack of sufficient funding, time to study, and the use of an inadequate method. Instead of the amount of dilution in mining studies, it is usually assumed to be a general improvement, such as 5% for huge and massive deposits, and 10% for small, tabular deposits. While these figures may be a good starting point in the early stages of mining studies, these numbers are not used in complex issues. In addition, the direct impact on short-term mining revenue and also the upswing have led to significant changes in other factors that in the long run lead to a reduction in the overall value of the project. For example, by reducing the effective capacity of the processing plant, the life of the mine will be prolonged. The dilution also reduces the grade of the input product and the output of the plant. In most cases, lower grade means less processing recovery. The dilution also increases cut-off grades, which in turn reduces the use of a mine's storage (Ebrahimi 2013).

The dilution in different mines varies according to the characteristics of the deposits, the operational and financial aspects of the economic boundary. For example, the shape of the ore, the height of the benches, the size of the equipment and the market conditions can affect the degree of dilution in a mine. In order to better produce a project, dilution studies should be considered as an inseparable part of any project.

1.1 The concept of dilution in mining operations

The dilution refers to waste materials that are mined from the minerals during the extraction process and combined with minerals, which reduce the final grade of minerals. These waste materials are combined with mineral matter and sent to the processing plant (Saeedi 2012).

In an inorganic block, the dilution occurs in two different regions; sometimes it is found in a block of minerals, waste or mineral in a very low grade, which is not possible to be separated, which is known as the inner dilution. The amount of internal dilution varies in different types of ore deposits. External dilution is referred to the waste that is extracted from the deposit and extracted from the mineral block. External dilution is based on geology, ore formation, drilling and blasting techniques, extraction operation scale and equipment size (Ebrahimi 2013). In Figure 1, the risk area is shown.

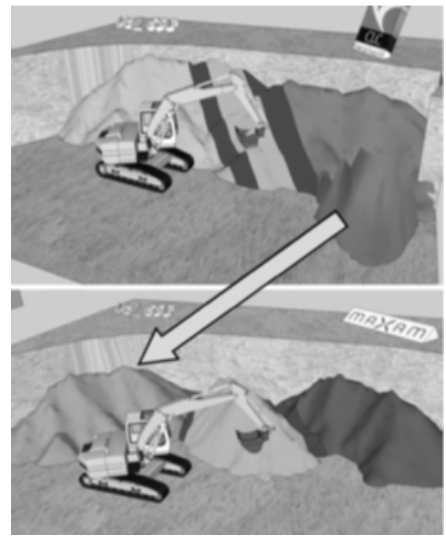

Figure 1. Risk area (Domingo *et al.* 2015).

The aim of the process of mine control is to maximise the amount of minerals extracted for processing or crushing for use in downstream products. This definition provides an understanding of the concepts of 'mine to factory' (Little 2015, Agoshkov *et al.* 1998).

2 THE BACKGROUND

Up to now, extensive research has been conducted in order to comprehensively understand and comprehend the dilution phenomenon. A study of the research conducted in addition to identifying the importance of the dilution problem, suggests that various factors can contribute to dilution. In 1966, an analytical model was presented by Augushkös with the assumption that valuable metals in precious minerals were found, valuable metal cassettes in the extruded materials and valuable metal cassettes in lateral rocks were associated with the dilution (Agoshkov *et al.*

1998). In 1986, Liuyong and Zhang Vijing devised studies on the economic destructive effects of dilution for thin vein conditions in tungsten mines in China, and provided some strategies to reduce dilution for these mining conditions (Yihong & Zhang 1986). In 2002, Ran presented a model for the development of open-source mining methods. In this model, the height of the workshop is considered as a beam, if the load rate is lower than the resistance, then in this case the workshop is unstable and, based on the depth of fall, the amount of dilution is calculated (Ran 2002). In 2003, Noppe presented a method for behavioural analysis, reporting and dilution control in coal underground mines (Noppe 2003).

In 2004, Chugh *et al*. considered a dilution model to study the impact of recovery on extraction speed, cost and profits from a tonne of coal mine in Illinois, USA. The model is a function of the thickness of the extraction layer, the thickness of the ceiling and the floor, the effect on the dilution, the specific gravity of the coal and the specific weight of the ceiling and the floor. This model assumes continuous production in such a way that the installation cycle and other cases do not cause any interruptions in the speed of the advance. It is also assumed that the average speed of cutting the coal and the lower and lower legs is the same (Chugh *et al.* 2004).

In 2005, Mubita conducted a research effort to reduce the rate of recovery and increase income in the Zambia Concola mine (Mubita 2005). In 2006, Soyer presented a method for estimating mineral depletion. The combination of mine design software and mine control systems has been used and aims to compare new methods of calculating dilution with old methods. The results of new methods used to estimate the amount of extractable minerals, 1.6% for tonnage, and 1.6% for grade, indicate the proximity to their actual values compared with the old methods (Soyer 2006). In 2007, Canada's Open Workshop mines provided numerical methods using Map3D software. In this method, the effects of parameters such as mining depth, workshop geometry, slope angle, tensions and their direction on the dilution have been investigated (Henning & Mitri 2007).

Also, in 2009 Saeedi *et al.* Using data collected from the Tabas coal mine and using the FLAC 2D software, provided a model for out-of-layer dilutions in longitudinal fuselage mines. In this modelling, the parameters affecting the dilution of the layer, including the depth of the mineral, the stress, the geometry of the ceiling immediately above the shale, and the quality of the roof and floor layer and the slope of the coal bed are considered (Saeedi *et al.* 2009). In 2011, Wigong Wang and colleagues conducted studies on the calculation and management of mineral waste and dilution under the conditions of three-dimensional technical visualisation. In their research, they introduced the principles of operation and the process of calculating mineral dissipation and dilution in the mining process, which is based on the adoption of geological models (Wang *et al.* 2011). The dilution control was studied by measuring the displacements in the explosion at the New Hamad AHFU gold mine in Ghana. The purpose of this study was to investigate the effect of explosion displacements on the control of its dilution and its reduction (Engmann *et al.* 2013).

In 2014, Tommila explored the effect of dilution profitability. The author believes that there are many reasons for the dilution, in fact, the reasons for the dilution are divided into three categories: 1- drilling and exploding; 2- errors in planning; 3- geotechnical problems (Tommila 2014). In the last quarter of 2015, an explosives classification system was dilution to control the degree to which classification of explosives can be classified and dilution based on this classification system (Little 2015). In 2019, Masoumi presented a self-correlated minimally-invariant invocative method for simulating continuous viable variables and the calculated dilution using this method based on lithology logs of the drill holes was a good result (Masoumi *et al.* 2019). Distribution of crushing and dilution size is effective on Asia's efficiency (Xingwana 2016). In the case of wet mining conditions due to incomplete and re-explosion, the mineralisation and tailings must be increased (Nikkhah & Taji 2018). For the control of the dilution of the Ajupa mine, an explosive displacement monitoring system was used which cost $116,031 during the study. The mine's revenue from the site was $866,869, indicating that the mining savings were due to an increase in control of $753,835 (Xingwana 2016). The direction and displacement of the explosion affects the cost of dilution and the process of mining to the plant (Rogers & Kanchibotla 2012; Gaunt *et al.* 2015). Dilution and loss of ore are important factors that can affect the cost and profitability of a mine. Considering the dilution is dependent on a number of factors that vary from period to period as a general rule, for larger periods, it might become easier. for estimate dilution, but the operation needs to deal with monthly, weekly or even daily production (Camara *et al.* 2018).

Marinin developed guidelines for assessing how losses and dilution indicators affect the cost chain from ore mining to processing. Economic evaluation method as a combination of factor analysis and engineering value, which saves operating costs. The basis of continuous planning is the analysis and control of the production process from the ore extraction stage to the refining of the mineral product (mine to mill). Based on the structure of the total reserves as well as the comparison between grade and metal performance due to changes in loss and dilution indices, the main results of the experimental study are that there is a reduction in mineral losses. Ore inventory changes in ore loss and dilution values (3.1% losses and 17% dilution in the baseline case scenario. 2.1% losses and 13.0% dilution under the project scenario) result in a 30 tonne reduction in processed ore values. The analysis of project sensitivity indicators shows that provided that the amount of ore mined and shipped fluctuates between 5%, the project efficiency of reducing the annual workload of mixing and loading ore varies in the range of $191.25-1147.5 (Marinin *et al.* 2021).

In open-cast extraction methods in porphyry mines, because of the high volume of extraction and the extent of the extractive operations front, dilution is due to several factors such as geological conditions and the presence of various dikes in minerals, design factors and engineering factors of operating factors, and the volume of buckets of loading machines and mine supervision. Given that the Sarcheshmeh copper mine is no exception to these conditions. Due to the fact that dilution is directly related to lowering the cost of producing and producing high-grade products, for this purpose, in this research, dilution has been studied in Sarcheshmeh copper mine.

3 THE EFFECT OF DILUTION IN MINING PROCESSES

The amount of dilution must be carefully measured and determined. Dilution control in active mines, which are in operation, are often controlled by a grade, which is the most controllable part of the mining profit. Mines are seeking to mechanise mine operations and increase production capacity to reduce costs and increase profits. Achieving these goals is only possible if you can maintain the degree of dilution. Operating mechanisation is always better than unmanaged and manual operations. But care should be taken that the cost savings in work will not be offset by increasing costs. The size and amount directly affect the economic profit of the mines, therefore, the calculation and management of the extent of the dilution as mine strategies are considered in the long run and are continuously studied and solved (Little 2015, Gaunt *et al.* 2015, Smith *et al.* 2015, Masoumi *et al.* 2019).

4 EFFECT OF DILUTION ON THE PROFITABILITY OF OPEN PIT MINES

Improvement affects profitability in two ways (Wang *et al.* 2011):

- Reduce direct costs by controlling more materials;
- Reduction of production (or product grade) with fixed factory capacity.

With higher dilution, the mineral is less processed, resulting in less crop production. The relationship between dilution and profitability can be illustrated in Figure 2.

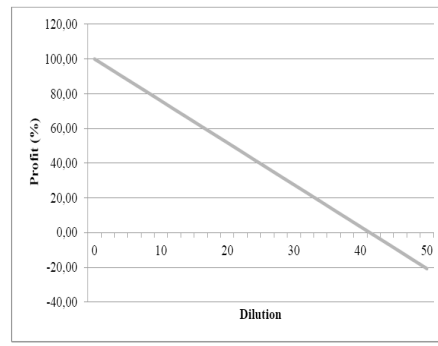

Figure 2. Impact of dilution on mining profit (Wang *et al.* 2011)

One of the consequences of a dilution is the reduction in the feed grade of the processing plant. A lower-grade feed means less income. On the borderline levels, the dilution may reduce the grade to the degree that it is for non-economic processing. In other words, the dilution may cause the mineral to be deposited (Saeedi *et al.* 2008).

5 STUDY OF DILUTION IN SARCHESHMEH COPPER MINE

Sarcheshmeh Copper Mine is one of the most important copper marble porphyry Mills in the world. The mine is located 160 km southwest of Kerman and 50 km southwest of Rafsanjan and at a height of 2600 meters above sea level. The mine is stocked with a margin of 0.25% and an average

Table 1. Dilution resources type in the Sarcheshmeh copper mine.

Dilution type	Dilution resources Sarcheshmeh Copper mine
Type 1. Dilution due to geometry	1. Dilution due to the interaction of ore deposit with the central dike 2. Dilution due to the loading machine bucket 3. Dilution due to waste rock in berm
Type 2. Dilution due to uncertainty in the knowledge of the *in situ* ore boundaries	4. Dilution due to mining development projects in ramps 5. Dilution due to geological conditions of the mine 6. Dilution due to uncertainty of block model
Type 3. Dilution due to blast movement	7 Dilution due to incomplete blast 8. Dilution due to back-break and side-break blasting block
Type 4. Dilution due to mining errors	9. Dilution due to the design of ore and waste blasting blocks in one blast 10. Spreading waste as a cover in the benchs and ramps 11. Colour similarity of ore with waste rock 12. Dilution due to cutting the floor of working benchs 13. Dilution due to reblast 14. Dilution due to instability of bench 15. Dilution due to mining operations at upper bench 16. Dilution due to waste stemming in production hole stemming 17. Dilution due to inadequate visibility of working night operator
Type 5. Dilution due to weather conditions	18. Undesirable weather conditions

grade of 0.66% and is 1763 million tons. In the development plan of the mine, the annual extraction of 25 million tons of minerals and 35 million tons of waste is set. Sarcheshme copper mine steps are 12.5 m and the width of the stairs is 8.75 m. Periodically and periodically, for each 4 steps, a large staircase with a width of 75.23 m is placed. The final slope of the mine wall is currently 34 to 36 degrees. Also, the width of the mine roads is 30 metres and the slope is 8% (Sarcheshmeh Copper Complex 2015).

5.1 Type and dilution control

In open pit mines dilution due geometry, dilution due uncertainty in knowledge of the *in situ* ore boundaries, dilution due blast movement, dilution due mining errors (Little 2015) and dilution due weather conditions.

Most of the production explosions in the Sarcheshmeh copper mine are of a bulk type for controlling the amount of explosive blocks that are multi-tile or mined or waste, the recovery rate is greater than the predicted value in the development plans, so that in explosions 7 and 10, the amount of dilution 13.17% and 10.45%, respectively. The main reasons for the development of this type of explosion are the non-explosion of mineral and tailings in the form of explosive separation and regeneration during loading due to mineral and tailings interlocking. If the detonator blast is used, along with the use of electronic detergents to control the development, it will be very effective. The sources of dilution in the Sarcheshmeh copper mine were classified into five categories and control and modification strategies (Table 1).

5.2 Database dilution control

In order to effectively investigate the dilution of Sarcheshmeh copper mine, the databases of drilling, blasting and loading sections were created as follows. The description of the database parameters is given in Table 2.

- Drilling Database: Including bench height, length, angle, and diameter of each hole, drilling pattern and total length drilling blast block.
- Blasting Database: Including burden, spacing, specific drilling, special charge, calculation of blast block dilution.
- Loading Database: Including performance, preparedness and movement of the loading machine (Nikkhah & Taji 2017), type and fuel of loading device and specific device.

Specific loading with the symbol (Slj), specific loading of the jth blasting block (hours per cubic

metre), which is calculated by dividing the total time available for loading machineries of jth blasting block (per hour) to the total volume of the j-th blasting block (cubic metre) (Taji *et al.* 2012). In Table 3 and Table 4, the data related to the drilling and exploding section and the loading section are presented.

Table 2. Description of collected parameters to create database.

Parameters	Symbol	Unit
Burden	B	m
Spacing	S	m
Diameter	D	inch
Hole length	H	m
Bench height	h_b	m
Sub-drilling	J	m
Stemming length	S_t	m
Ratio of length to width of blast block	R_{LW}	-
Volume of blast block	V_b	m^3
Blast block tonnage	T_b	ton
Specific drilling	S_d	m/m^3
Specific charge	S_c	kg/m^3
Loading specific	S_l	m^3
Dilution	D_i	%
Blast block tonnage ore	T_{or}	ton
Blast block tonnage waste	T_{wa}	ton

6 DILUTION MODELLING

Studies in previous sections show that many parameters can be effective in dilution. But these parameters were ranked so that the control could be controlled and reduced. For this purpose, the data was studied using Spss v.21 software. By studying the dependent and independent parameters, one can get the relationship between each one together and get informed about the process of their changes. This helps to compare the accuracy and overall trend of the changes with the theories proposed in the dilution prediction. Also, different linear and nonlinear models have been tested and selected by using two Watson Camera and F-model tests. To compare the accuracy of nonlinear regression prediction, F test was used. In this test, if the Sig value obtained at 95% confidence level is less than 5%, it is indicative that the accuracy of the estimate for the obtained relationship is acceptable. Also, in the Watson camera test, the value obtained is between 0-4. The predicted model is acceptable (Mirzadeh 2010). In Table 5, the matrix of the correlation coefficients of the studied parameters are show.

Table 3. Database unit drilling and blasting 7 blast blocks.

Parameters	symbol	Unit	Range
Burden	B	m	5-7
Spacing	S	m	6-9.5
Diameter	D	inch	6.5-10
Hole length	H	m	14.5-15
Bench height	h_b	m	12.5
Sub-drilling	J	m	2.5
Stemming length	S_t	m	6.5-8.5
Ratio of length to width of blast block	R_{LW}	-	1.36-4.95
Volume of blast block	V_b	m^3	67718.04-412139.77
Blast block tonnage	T_b	ton	48000-108438

The values of the correlation coefficients shown in Table 6 are variables in the range 1 to 1. The positive sign of these coefficients expressing the direct relationship with the negative sign expressing their inverse relationship with each other and their magnitude indicates their effect. The coefficients of greater absolute magnitude have a higher impact and therefore have a stronger relationship. The coefficients in the matrix diameter are usually 1. Since the relationship of each variable with itself is a completely linear relationship. The same is true of the matrix.

Table 4. Key database 7 blast blocks.

Parameters	Symbol	Unit	Range	Average
Specific drilling	S_d	m/m^3	0.013-0.04	0.021
Specific charge	S_c	kg/m^3	0.256-0.612	0.446
Specific loading	S_l	m^3	0.004-0.009	0.007
Dilution	D_i	%	0.000-13.7	6.73

Table 5. Matrix of correlation coefficients.

		B	S	D	H	J	St	R_{LW}	S_d	S_c	S_l	D_j
B (m)	Pearson correlation	1	0.945**	0.941**	-0.411	-0.411	0.239	0.059	-0.700	0.590	-0.481	0.383
	Sig. (2-tailed)		0.001	0.002	0.359	0.359	0.606	0.900	0.080	0.163	0.275	0.397
	N	7	7	7	7	7	7	7	7	7	7	7
S (m)	Pearson correlation	0.945**	1	0.877**	-0.255	-0.255	0.416	-0.045	-0.817*	0.469	-0.570	0.638
	Sig. (2-tailed)	0.001		0.010	0.581	0.581	0.353	0.923	0.025	0.289	0.182	0.123
	N	7	7	7	7	7	7	7	7	7	7	7
D (inch)	Pearson correlation	0.941**	0.0877**	1	-0.250	-0.250	0.404	0.018	-0.498	0.432	-0.415	0.351
	Sig. (2-tailed)	0.002	0.010		0.589	0.589	0.369	0.970	0.255	0.333	0.354	0.440
	N	7	7	7	7	7	7	7	7	7	7	7
H (m)	Pearson correlation	-0.411	-0.255	-0.250	1	1.000**	0.527	-0.547	0.465	-0.846*	-0.248	0.389
	Sig. (2-tailed)	0.359	0.581	0.589		0.000	0.224	0.203	0.294	0.017	0.592	0.389
	N	7	7	7	7	7	7	7	7	7	7	7
J (m)	Pearson correlation	-0.411	-0.255	-0.250	1.000**	1	0.527	-0.547	0.465	-0.846 *	-0.248	0.389
	Sig. (2-tailed)	0.359	0.581	0.589	0.000		0.224	0.203	0.294	0.017	0.592	0.389
	N	7	7	7	7	7	7	7	7	7	7	7
St (m)	Pearson correlation	0.239	0.416	0.404	0.527	0.527	1	-0.003	-0.200	-0.141	-0.620	.787*
	Sig. (2-tailed)	0.606	0.353	0.369	0.224	0.224		0.995	0.667	0.763	0.138	0.036
	N	7	7	7	7	7	7	7	7	7	7	7
R_{LW}	Pearson correlation	0.059	-0.045	0.018	-0.547	-0.547	-0.003	1	-0.225	0.625	-0.193	-0.206
	Sig. (2-tailed)	0.900	0.923	0.970	0.203	0.203	0.995		0.628	0.133	0.679	0.657
	N	7	7	7	7	7	7	7	7	7	7	7
S_d (m/m)	Pearson correlation	-0.700	-0.817*	-0.498	0.465	0.465	-0.200	-0.225	1	-0.595	0.516	-0.596
	Sig. (2-tailed)	0.080	0.025	0.255	0.294	0.294	0.667	0.628		0.159	0.236	0.158
	N	7	7	7	7	7	7	7	7	7	7	7
S_c (kg/m)	Pearson correlation	0.590	0.469	0.432	-0.846 *	-0.846 *	-0.141	0.625	-0.595	1	-0.155	-0.026
	Sig. (2-tailed)	0.163	0.289	0.333	0.017	0.017	0.763	0.133	0.159		0.740	0.957
	N	7	7	7	7	7	7	7	7	7	7	7
S_l (hr/m)	Pearson correlation	-0.481	-0.570	-0.415	-0.248	-0.248	-0.620	-0.193	0.516	-0.155	1	-0.727
	Sig. (2-tailed)	0.275	0.182	0.354	0.592	0.592	0.138	0.679	0.236	0.740		0.064
	N	7	7	7	7	7	7	7	7	7	7	7
D_j (%)	Pearson Correlation	0.383	0.638	0.351	0.389	0.389	0.787*	-0.206	-0.596	-0.026	-0.727	1
	Sig. (2-tailed)	0.397	0.123	0.440	0.389	0.389	0.036	0.657	0.158	0.957	0.064	
	N	7	7	7	7	7	7	7	7	7	7	7

**. Correlation is significant at the 0.01 level (2-tailed).

*. Correlation is significant at the 0.05 level (2-tailed).

Table 6. Proposed models and analysis of variance of projected desalination models with independent parameters.

Predict model	
1	$Dilution = -81.163 + 30.332\log S_t - 30.418\log R_{LW} - 7.962\log S_d$
2	$Dilution = -88.247 + 33.282\log S_t - 7.236\log S_d$
3	$Dilution = 284.354 - e^{275.412 S_d} + e^{0.002 S_t}$
4	$Dilution = -5.989 + 0.273 S_t^{\,2} - 4791.127 S_d^{\,2}$

Analysis of variance (ANOVA)

Model No.	R	R^2	Adj. R^2	Std. error	F change	Sig F change	Durbin-Watson
1	0.988	0.977	0.953	0.949	41.928	0.006	2.159
2	0.937	0.877	0.877	1.878	14.281	0.02	1.654
3	0.892	0.796	0.796	2.431	7.816	0.04	2.335
4	0.915	0838	0.757	2.168	10.333	0.03	2.258

Table 7. Multivariate nonlinear regression coefficients and statistical parameters of coefficients for models 1, 2, 3, and 4.

Model No.	Independent variables	Unstandardised coefficients		Standardised coefficients	95% Confidence interval for B		t values	Collinearity statistics	
		B	Std. Error	Beta	Lower Bound	Upper Bound		Tolerance	VIF
1	Constant	-81.163	9.460		-111.270	-51.056	-8.579		
	S_t	30.332	4.420	0.621	16.267	44.397	6.863	0.948	1.055
	R_{LW}	-3.418	0.955	-0.325	-6.456	-0.380	-3.581	0.944	1.059
	S_d	-7.962	1.173	-0.613	-11.694	-4.230	-6.789	0.953	1.05
2	Constant	-88.247	18.398		-139.327	-37.166	-4.797		
	S_t	33.282	8.635	0.682	9.307	57.258	3.854	0.982	1.018
	S_d	-7.236	2.297	-0.577	-13.613	-0.858	-3.150	0.982	1.018
3	Constant	284.534	116.443		-38.944	607.652	2.442		
	S_t	-275.412	113.729	-0.558	-59.173	40.349	-2.422	0.959	1.042
	S_d	0.002	0.001	0.593	0.000	0.04	2.574	0.959	1.042
4	Constant	-5.989	5.385		-20.940	8.961	-1.112		
	S_t	0.273	0.090	0.627	0.022	0.523	3.021	0.941	1.063
	S_d	-4791.127	1870.645	-0.532	-9984.869	402.616	-2.561	0.941	1.063

Table 8. Proposed models and analysis of variance of suggested dilution models with independent parameters.

Predict model	
1	$Dilution = -91.238 + 35.679\log S - 18.144\log D + 30.559\log$
2	$Dilution = -18.627 - 0.155 D^2 + 0.253 S_*^{\,2} + 0.326 S^2$

Analysis of variance (ANOVA)

Model No.	R	R^2	Adj. R^2	Std. error	F change	Sig F change	Durbin-Watson
1	0.985	0.970	0.939	1.082	31.815	0.009	2.228
2	0.999	0.999	0.997	0.230	728.994	0.000	1.765

Table 9. Multivariate nonlinear regression coefficients and statistical parameters of coefficients for models 1 and 2.

Model No.	Independent variables	Unstandardised coefficients		Standardised coefficients	95% Confidence interval for B		t values	Collinearity statistics	
		B	Std. Error	Beta	Lower Bound	Upper Bound		Tolerance	VIF
1	Constant	-91.238	10.599		-124.968	-57.508	-8.608		
	S	35.679	5.875	1.282	16.982	54.376	6.073	0.228	4.388
	D	-18.144	4.05	-0.936	-31.208	-5.08	-4.420	0.227	4.411
	S_t	30.559	5.389	0.626	13.407	47.711	5.670	0.834	1.199
2	Constant	-18.627	0.573		-20.450	-16.803	-32.506		
	D	-0.155	0.007	-1.024	-0.176	-0.134	-23.249	0.235	4.249
	S_t	0.253	0.01	0.584	0.220	0.285	24.411	0.806	1.241
	S	0.326	0.011	1.353	0.291	0.360	30.242	0.228	4.383

Among the parameters mentioned, the length of the choral flowering fabric with a correlation coefficient of 0.957 had the highest effect and the weight ratio with the coefficient of correlation of 0.204 had the least effect on the dilution.

6.1 Relationship between S_d, R_{LW} AND S_t with dilution

In order to investigate the effect of effective parameters on dilution, using multi-parameter linear and non-linear regression, four models were obtained in Table 7 of the models.

In order to control the validity of the models, or in other words, to control its significance, the error independence test was used from the Watson camera and the F test. The results of both tests are shown in Table 6. Since the value of both tests is acceptable at the 95% confidence level, the correlation coefficient of the obtained models for dilution indicates that the dilution parameter has a significant relation with its independent variables at a suitable level. This test is another basis for determining the validity of the model.

Variable inflation factor has been used to confirm the lack of relation between independent input variables. So that the variance inflation factor for each independent variable is less than 10. This means that there is no significant correlation between the independent input variables (Faramarzi *et al.* 2013). The variance inflation factor results for the models 1, 2, 3, and 4 are shown (Table 7).

6.2 Relation between spacing, diameter and stemming with dilution

In the analysis of nonlinear regression, logarithmic and invariant variables of hole spacing, diameter of chalk and clipping length were considered as independent variable and dilution of dependent variable. Two models 1 and 2 were proposed, as indicated in Table 8.

Accordingly, the correlation coefficient of 0.970 and 0.999, respectively, for the dilution models 1 and 2, show a significant correlation between the dilution parameter and its independent variables, which is also the basis for determining the validity of the model. According to the variance inflation factor test, the independent variables of model 1 and 2 are presented in Table 9. There is no solid correlation between the independent input variables of models 1 and 2.

In the proposed models, according to the standardised coefficient column (Borcard 2002), it can be seen that the standardised coefficients of applying regression by evaluating this column can be concluded which factor has a positive effect and which negative effect is the diameter of the chamber, the special drilling and the length to width ratio The explosive block reduces depletion, but the length of the flowering and the spacing will increase it. Since the values of their standard coefficients were the highest values.

7 CONCLUSIONS

In this research, the study of dilution was investigated in Sarcheshmeh copper mine. Most of the explosions are of precise type flare explosions. According to the calculations, the highest dilution rate in the Sarcheshmeh copper mine is 13.17, and the average dilution is 6.73. In order to study the effective parameters on dilution, we used statistical analysis. The very high correlation coefficient of the obtained models indicates the effect of independent parameters on dilution. By comparing the results, we find that stemming length, spacing, hole diameter and specific drilling are the most important parameters affecting dilution. By controlling some of the parameters that affect the dilution, the changing of blasting pattern design can minimise the amount of

dilution, which will result in profitability and mining costs reduction in Sarcheshmeh Copper Complex.

8 ACKNOWLEDGMENTS

The authors appreciate Iranian copper industry national company.

REFERENCES

Agoshkov, M., Borisov, S. & Boyarski, V. 1998. Mining of ores and non-metalic minerals (Trans. V. Kochin), *Mir Publishers Moscow*, Russia.

Borcard, D. 2002. Multiple and partial regression and correlation Partial r^2, contribution and fraction, *Université de Montréal Département de sciences biologiques*, Canada.

Chugh, Y. P., Moharana, A. & Patwardhan, A. 2004. An analysis of the effect of out-of-seam dilution on coal utilisation, *International Conference on Clean Technologies for the Mining Industry, University of Concepción,* Chile.

Camara, T.R., Leal, R.S., Peroni., R.L. & Capponi, L.N. 2018. Controlling operational dilution in open-pit mining, *Mining Technology, DOI: 10.1080/25726668.2018.1470275*.

Domingo, J.F.D., Leite, F.S., Mirada, V.G. & Carrasco, I.C. 2015. Dilution, ore grade and blast movement calculation model, *Proc. Of FRAGBLAST 11, Fragmentation by blasting.*

Ebrahimi, A. 2013. An attempt to standardise the estimation of dilution factor for open pit mining project, *World Mining Congress, Montreal*, Canada.

Engmann, E., Ako, S., Bisiaux, B., Rogers, W. & Kanchibotla, S. 2013. Measurement and modelling of blast movement to reduce ore losses and dilution at Ahafo gold mine in Ghan, *Ghana Mining Journal* 27-36.

Faramarzi, F., Mansouri, H. & Ebrahimi Farsangi, M.A. 2013. A rock engineering systems-based model to predict rock fragmentation by blasting, *International Journal of Rock Mechanics and Mining Sciences* 60: 82-94.

Gaunt, J., Symonds, D., McNamara, G., Adiyansyah, B., Kennelly, L., Sellers, E.J. & Kanchibotla, S.S. 2015. Optimisation of drill and blast for mill throughput improvement at Ban Houayxai mine, *Proc. Of FRAGBLAST 11, Fragmentation by blasting.*

Henning, J. G. & Mitri, H. S. 2007. Numerical modelling of ore dilution in blasthole stoping, *International Journal of Rock Mechanics & Mining Sciences* 44: 692-703.

Little, T.N. 2015. Classification and development in grade control blasting for surface mines, *Proc. Of FRAGBLAST 11, Fragmentation by blasting.*

Masoumi, I., Kamali, G.R. & Asghari, O. 2019. Assessment of an ore body internal dilution based on multivariate geostatistical simulation using exploratory drill hole data, *Journal of Mining and Environment (JME)* 10(1): 271-286.

Mirzadeh, M. R. 2010. Statistical analysis with SPSS, *Teheran, Taymaz Pub*.

Mubita, D.M. 2005. Recent initiatives in reducing dilution at Konkola mine, Zambia, *Journal-South African Institute of Mining and Metallurgy* 105(2):107-112.

Marinin, M., Marinina, O. & Wolniak, R. 2021. Assessing of losses and dilution impact on the cost chain: case study of gold ore deposits, *Journal of Sustainability, DOI:* doi.org/10.3390 /su13073830.

Najafi, B., Saeedi, G.S. & Ebrahimi Farsangi, M.A. 2014. Risk analysis and prediction of out-of-seam dilution in longwall mining, *International Journal of Rock Mechanics & Mining Sciences* 70: 115–122.

Nikkhah, A. & Taji, M. 2017. Investigating the impacts of fragmentation caused by blasting operation on machinery efficiency of Sarcheshmeh Copper Mine, *Journal of Research-Papers Mineral Resources Engineering* 28: 267-272.

Nikkhah, A. & Taji, M. 2018. The effect of the underground water on production costs and mining operation in open-pit mines, Case Study, *Sarcheshmeh Copper Mine* 28: 267-272.

Noppe, M. 2003. The measurement and control of dilution in an underground coal operation, *5th International Mining Geology Conference, Bendigo, Australia*.

Ran, J. 2002. Hangingwall sloughing mechanism in open stope mining, *CIM Bulletin* 95: 74-77.

Rogers, W.D. & Kanchibotla, S.S. 2012. Application of stochastic approach to predict blast movement, *Proceedings of the 10th international symposium rock fragmentation by blasting, New Delhi,* India.

Saeedi, G., Rezai, B., Shareiar, K., Oraee, K. 2008. Quantifying level of out-of-seam dilution for longwall mining method and its impact on yield of coal washing plant in Tabas coal mine, *Proceedings of the International Seminar on Mineral Processing Technology, Trivandrum,* India.

Saeedi, Gh. 2012. Dilution control in mines. *Ministry of Industry*, Mine and Trade, Office of Oversight and Utilisation of Mining Rules and Standards.

Sarcheshmeh Copper Complex 2015. Report of Sarcheshmeh copper mine development plan, *Sarcheshmeh Copper Mine Engineering, Design Department.*

Smith, C.B., Nehring, M. & Bosompem, M.K. 2015. A critique of selective mining unit sizing at Century Mine to optimise productivity with dilution, *Proc. Of FRAGBLAST 11, Fragmentation by blasting*.

Soyer, N. 2006. An approach on dilution and ore recovery/ loss calculations in mineral reserve estimations at the Cayeli mine, Turkey, *A Thesis submitted to the Graduate School of Natural and Applied Sciences of Middle East Technical University.*

Taji, M., Ataei, M., Goshtasbi, K. & Osanloo M. 2012. A new approach for open pit mine blasting evaluation, *Journal of Vibration and Control* 2(3): 25-36.

Tommila, E. 2014. Mining method evaluation and dilution control in Kittilä mine, *Master's Thesis.*

Wang, W., Huang, S., Wu, X. & Ma, Q. 2011. Calculation and management for mining loss and dilution under 3D visualisation technical condition, *Journal of Software Engineering and Applications* 4: 329-334.

Xingwana, L. 2016. Control of ore loss and dilution at AngloGold Ashanti, Iduapriem Mine using blast movement monitoring system, *Ghana Mining Journal* 16 (1): 49-59.

Xingwana, L. 2016. Monitoring ore loss and dilution for mine-to-mill integration in deep gold mines: a survey-based investigation, *Southern African Institute of Mining and Metallurgy* 116(2): 149-160.

Yihong, L. & Zhang, W. 1986. Reducing waste-rock dilution in narrow-vain conditions at tungsten mines in China, *Mining Science and Technology* 4: 1-7.

Maastricht Conference Proceedings 2022, R. Holmberg et al

Understanding single salt, dual salt, and multiple salt bulk emulsions and emulsion blends

D.S. Scovira, B. Victor & Q. Steyl
BME, a division of Omnia Group (Pty) Ltd, Gauteng, South Africa

ABSTRACT: Bulk emulsions and emulsion blends may be formulated with a single salt, dual salts, or multiple salts. Single salt bulk emulsions and emulsion blends, based on ammonium nitrate, are familiar to many blasting professionals as they are manufactured and employed on a global basis. Blasting professionals may be less acquainted with dual and multiple salt emulsion and emulsion blends that may include calcium nitrate, sodium nitrate, and urea in their formulations.

1 INTRODUCTION

Bulk emulsions and emulsion blends may be formulated with a single salt, dual salts, or multiple salts. Single salt bulk emulsions and emulsion blends, most based on ammonium nitrate, are familiar to many blasting professionals as they are manufactured and employed on a global basis. Blasting professionals may be less acquainted with dual and multiple salt emulsion and emulsion blends that may include calcium nitrate, sodium nitrate, and urea in their formulations. These additional salts can impart various beneficial qualities to address end user needs and blasting results.

2 EMULSION STABILITY AND CRYSTALLISATION

The process of heterogenous seed driven crystallisation primarily effects single salt bulk emulsions. Seed needle crystal grows and

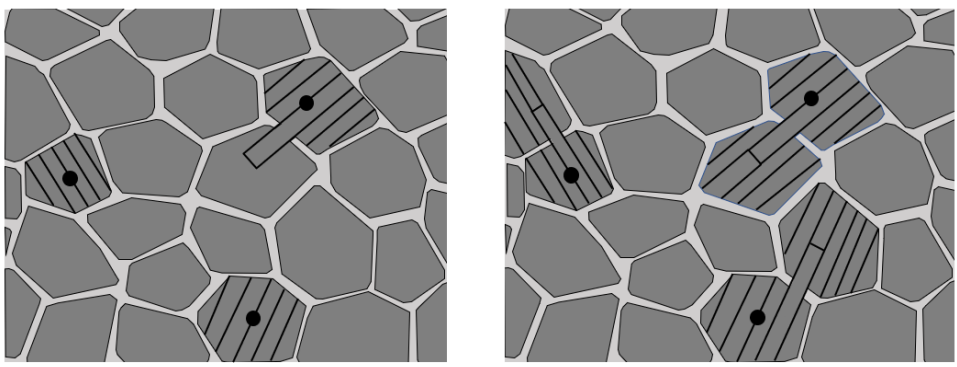

Figure 1. Heterogenous (seed) driven crystallisation in a AN single salt emulsion.

penetrate adjacent oxidiser phase cells. The compromised oxidiser cell crystallises. The cycle repeats and eventually compromises the emulsion. The result is commonly called ‘salting out’ or ‘phase separation’. See Figure 1 - Heterogenous (seed) driven crystallisation.

Dual and multiple salt emulsions are inherently chemically resistant to heterogenous seed driven crystallisation. Dual ANCN salt emulsions have a chemistry advantage over single salt AN emulsions in keeping the AN in solution. The crystallisation point is depressed due to increased solubility, and this stabilises the oxidiser phase. Crystals in the oxidiser phase of dual salt ANCN emulsion are cubic and less likely to form needles. Accordingly, they are less likely to drive the homogenous seed crystallisation process previously described. See Figure 2 – Dual salt emulsion cubic crystals.

Sodium nitrate ($NaNO_3$, SN) is also a salt that is also used in multiple salt emulsion formulations. Sodium nitrate is commonly found in detonator sensitive packaged emulsion formulations and some bulk emulsions aimed at small diameter applications. Specific to packaged products, sodium nitrate does not introduce water to the emulsion composition and contributes to keeping the total emulsion water content low enough to ensure detonator sensitivity. Specific to small diameter bulk emulsion products, lesser amounts of sodium nitrate addition be used to enhance sensitivity without crossing the threshold of detonator sensitivity. During manufacture, sodium nitrate acts as a eutectic that depresses the crystallisation temperature (fudge point) and results in stable finished emulsion high in energetic salt content and low water content.

Dual salt ANCN emulsion technology is also commonly called ‘cold emulsion technology’. The meaning behind cold emulsion technology is that the emulsion matrix is manufactured at a lower temperature of 65℃ versus 85℃ [149℉ versus 185℉] for a single salt AN emulsion. CN promotes emulsification and therefore less emulsifier is required for stable emulsion formation.

Dual salt ANCN emulsions have a finished temperature of 50℃ [122℉] and no cooling time is required before field use. The lower manufacturing temperature eliminates the need for additional storage capacity at the plant to allow

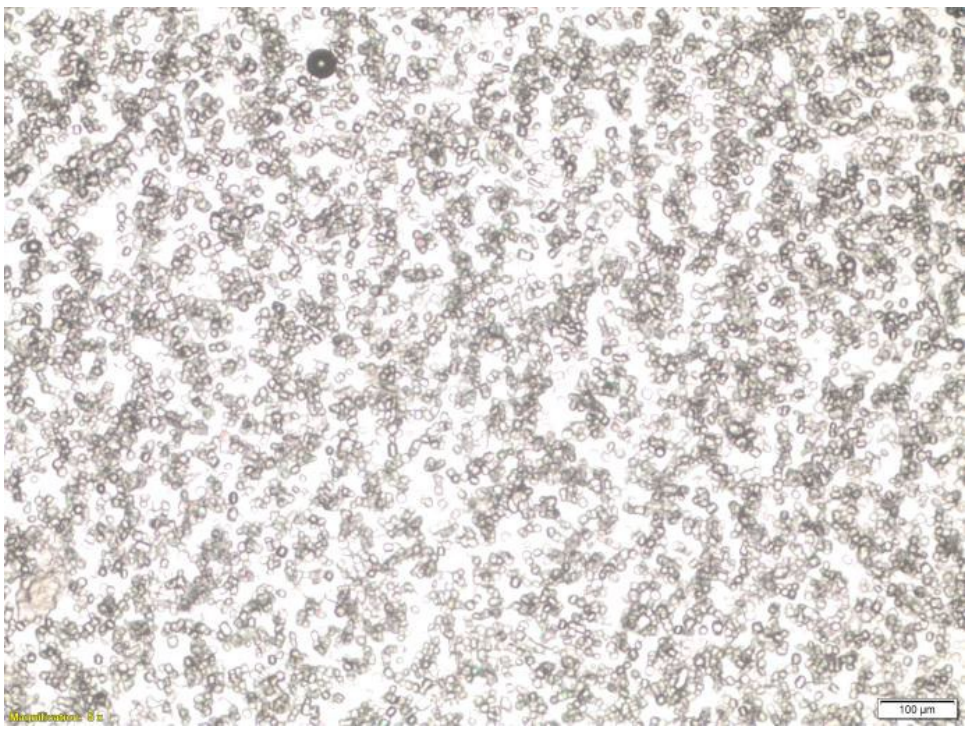

Figure 2. Electron microscope image of cubic crystals of a dual salt and water solution.

enough product cooling time before use. The lower manufacturing temperature also requires less energy intensity and cost at the plant.

In remote mining locations, where installation of a bulk emulsion manufacturing plant is not economically justified or desired, bulk emulsion products may need to be delivered over considerable distances and stored and consumed over extended periods of time. Dual and multiple salt emulsions are highly stable and have been demonstrated to resist oxidiser and fuel phase separation during the rigor of transport, resistance to breakdown by repeated re-pumping, and salting out during extended storage times.

3 OXYGEN BALANCE AND POST BLAST FUME

Oxygen balance (OB, or OB%) is the term used to indicate the degree that an explosive can be oxidised. If an explosive contains sufficient oxygen to form only CO_2, H_2O and N_2, then the explosive is at zero oxygen balance. Due to chemical reaction kinetics, the detonation of explosives based on nitrogen molecules may generate toxic fumes of nitrogen dioxide (NO_2), nitric oxide (NO), and carbon monoxide (CO).

Oxygen balance has an influence on the detonation products and is illustrated by the following reactions: See Equation 1 and Equation 2: Negative and positive oxygen balances.

Negative oxygen balance (Excess fuel):
$2NH_4NO_3 + CH_2 \rightarrow 2N_2 + CO + 5H_2O$
Equation 1.

Positive oxygen balance (Excess oxidiser):
$5NH_4NO_3 + CH_2 \rightarrow 4N_2 + CO_2 + 11H_2O + 2NO$
Equation 2.

Figure 3 is an illustration of NOx production with AN/fuel blends (ANFO) with increasing oxygen balance. It can be seen from the figure that NO_x production is rapidly increased and most affected by excess oxidiser (oxygen positive). It is therefore vital when formulating an emulsion explosive that there is enough oxygen for the available fuel. See Figure 3, the relationship of oxygen balance to NOx.

When looking at the actual percentage of oxygen in ammonium nitrate versus calcium nitrate there is not much of a difference:

% Oxygen in NH_4NO_3 = 59.97%
% Oxygen in $Ca(NO_3)_2$ = 58.51%

However, when looking at the oxygen balance of ammonium nitrate versus calcium nitrate, it is shown that calcium nitrate contributes more than twice as much to the oxygen balance than ammonium nitrate does:

OB% = -1600/molecular weight x (2x +(y/2) + m-z). Where: x = number of atoms of carbon(C); y = number of atoms of hydrogen (H); m = number of atoms of metal (metallic oxide produced); and z = number of atoms of oxygen (O).

Oxygen balance for NH_4NO_3 = +0.20 (+20%)
Oxygen balance for $Ca(NO_3)_2$ = + 0.49 (+49%)

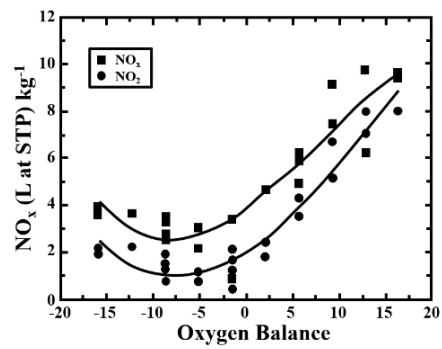

Figure 3. Relationship of Oxygen balance to NOx generation.

This results in ANCN dual salt emulsions formulations being more closely oxygen balanced as compared to single salt AN emulsions. In field practice, single salt AN bulk emulsions and bulk emulsion blends have been observed to generate considerable post blast NOx fume while dual salt ANCN bulk emulsions and emulsion blends have been noted to produce lesser degrees of NOx.

The low finished product temperature of dual salt ANCN emulsions may also reduce the heat erosion of AN prill in emulsions blends and this can also aid in reducing post blast NOx fume.

4 AMMONIA AND NITRATE IN MINE WATER

Chemical contents of mine water discharged to the environment continues to draw attention and additional regulation. NH_4^+ (ammonium or ionised ammonia) is essentially harmless to marine life; NH_3^0 (un-ionised or free ammonia) is known to be toxic to marine life. Ammonia and nitrate ions have been shown to be especially harmful to fish

and fish eggs. Very low levels have been shown to consequential and hence the mine water discharge can be highly monitored by regulators. Many mines are required to capture and/or treat their mine wastewater before discharge to the outside environment. In Canada, the Metal and Diamond Mining Effluent Regulations (MDMER) effective 01 June 2021 established a federal effluent limit of unionised ammonia at a monthly mean concentration limit of 0.5 mg-N/L [0.5 ppm].

Residual bulk emulsions or emulsion blends originating from product that migrates into cracks/voids in the blast hole, occurs as spillage at the collar of the hole, and other causes may end up in blasted rock. In Canada, the US Pacific Northwest, and other wet-dry-wet cyclical environments, muck piles and waste rock may be repeatedly washed by rain and melting snow between dry periods. This wet-dry-wet cycling environment promotes decomposition of the emulsion with subsequent leaching out of the component salts into the mine water.

Regarding bulk explosive applications in sensitive/regulated areas, consider the differences for the two compositions of emulsions if broken down and then dissolved in water. Broken down emulsion results in the liberation of NH_4^+. Liberated NH_4^+ from emulsion when introduced to environmental water, and dependent upon environmental water pH and temperature, can be converted to NH_3^0. Equation 3 shows the ammonium-ammonia equilibrium.

$NH_3 + H_2O \leftrightarrow NH_4^+ + OH^-$
Equation 3.

The Iowa Calculator can be used to determine the NH_3^0 amount created/present based on water pH and temperature.

The following example is presented for unionised ammonia at a limit of 0.5 mg/L or 0.5 ppm and compares industry standard AN single salt emulsion with an ANCN dual salt emulsion formulations. Both emulsions contain a total of 76% oxidiser salts. Assume that the salts from the emulsion oxidiser phase are fully broken down/fully separated from the fuel phase and other components of the emulsion. The single salt AN emulsion contains 17.17% NH_4+ and the dual salt ANCN emulsion contains 10.23% NH_4+. This equates to a 6.94% difference in the NH_4^+ quantity.

One kilogram of broken down AN emulsion can release 171 700 mg [0.38 lb] of NH_4^+ to the environment = 171 700 ppm. One kilogram of broken down ANCN emulsion can release 102 300 mg [0.23 lb] of $NH4^+$ to the environment. = 102 300 ppm. This is a +67.84% difference in NH_4^+ release.

If the above ammonium quantities are dissolved in 1 litre of water, then:

1 kg [2.204 lb] AN emulsion can result in 679 mg [0.0015 lb] of NH_3^0 (679 ppm, 679 mg/l [0.0057 lb/gal]) released in water at pH 7 at temperature of 20°C.

171700	**Enter:** Total (NH3+NH4)-Nitrogen Concentration (mg/L)
7	**Enter:** pH
20	**Enter:** Temperature (degrees C)
678.889738075	**Free Ammonia-Nitrogen Concentration** (mg/L)

(679 mg/l) / 0.5 ppm = 1358 litres [358.75 gal] of water required to dilute to 5 ppm concentration. [0.0057 lb/gal]

1 kg [2.204 lb] of ANCN emulsion can result in 405 mg [0.001 lb] of NH_3^0 (405 ppm, 405 mg/l [0.0034 lb/gal]) released in water at pH 7 at temperature of 20°C.

102300	**Enter:** Total (NH3+NH4)-Nitrogen Concentration (mg/L)
7	**Enter:** pH
20	**Enter:** Temperature (degrees C)
404.487013425	**Free Ammonia-Nitrogen Concentration** (mg/L)

(405 mg/l) / 0.5 ppm = 810 litres [214.98 gal] water required to dilute to 0.5 ppm concentration. [0.0034 lb/gal]

Therefore, it takes + 71.5% more water to dilute 1 kilogram [2.204 lb] of disassociated single salt AN emulsion down to 0.5 ppm concentration as compared to 1 kilogram of disassociated dual salt ANCN emulsion.

By design, some mining and dumping operations are constructed so that the mine water drains into a central pit lake. This pit lake water gets treated and helps to avoid the issue of discharge release 'pulses' that can be caused by periods of dry (where emulsion breaks down) followed by periods of wet (broken down emulsion washes out). Scrubbing out ammonia and nitrate from mine discharge water may be done by chemical treatment, filtering, and/or bioremediation, and these treatments of large quantities of mine discharge water can be costly.

There is no significant difference to the nitrate (NO_3-) quantity liberated when comparing single salt AN emulsions to dual salt ANCN emulsions.

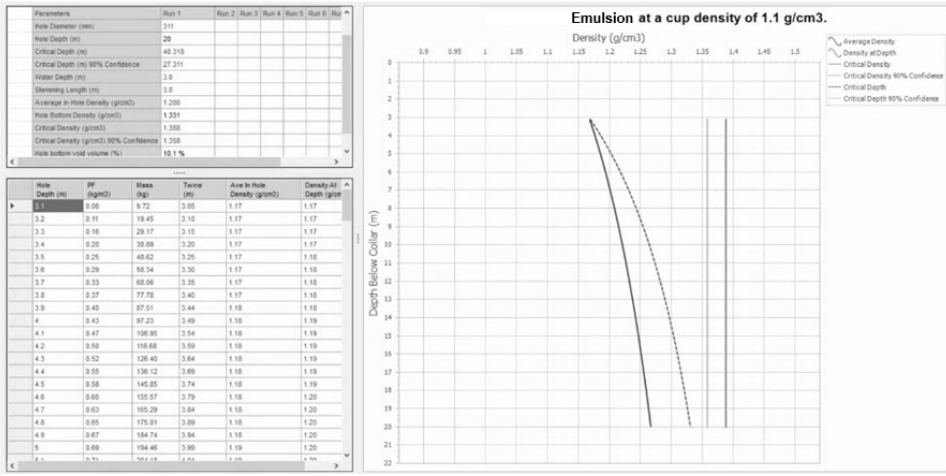

Figure 4. Example of critical density and void space calculation from BME's DensDepth™ program.

The single salt AN emulsion contains 59.03% NO_3- and the dual salt ANCN emulsion contains 59.44% NO_3-

5 CRITICAL DENSITY AND VOID SPACE FOR GASSED EMULSIONS

To realise reliable performance and optimal results with gas sensitised single salt, dual salt, and multiple salt emulsions and emulsion blends, it is important to understand the relationship between hole diameter, product densities, and maximum hole depth. This relationship must be understood by the user to ensure there is enough critical void space in the bulk product at the bottom of the hole to ensure detonation sensitivity. To operate in the clear of exceeding critical densities, many manufacturers/suppliers of gassed bulk emulsions have computer programs to aid in the calculation of the relationship using site specific conditions. By manipulating the cup density, the end user can be ensured that there is sufficient critical void space and that the critical density is not exceeded for the drilled hole diameter and depth. See Figure 4, an example of critical density and void space calculation.

6 ENERGY VALUES AND IDEAL DETONATION CODE

Manufacturers set standard ANFO to a Relative Weight Strength (RWS) = 100 and Relative Bulk Strength (RBS) = 100. The ANFO RWS and RBS are typically published to establish baseline values on each manufacturer's Technical Data Sheet (TDS). A literature search shows that the Absolute

Table 1. Survey of standard ANFO and Ideal Detonation Codes – 2019.

Manufacturer or Reference	Code Name	ANFO Density (g/cc)	Energy Published	Absolute Weight Strength (AWS)	Absolute Bulk Strength (ABS)	Cutoff Pressure
Company A - Global	Ideal Code A	0.80	3.82 MJ/kg	913 cal/g	730 cal/cc	100 MPa
Company B - Global	Ideal Code B	0.78 - 0.82	2.3 - 2.5 MJ/kg	574 cal/g	459 cal/cc	100 MPa
Company C - Region 1	Not Stated	0.80	2260 kJ/kg	540 cal/g	432 cal/cc	Not Stated
Company C - Region 2	Ideal Code C	0.84	890 kcal/kg	890 cal/g	748 cal/cc	Not Stated
Company D - Global	Ideal Code D	0.80	2.30 MJ/kg	550 cal/g	440 cal/cc	100 Mpa
Company E - Global	Ideal Code E	0.82	720 cal/cc, 880 cal/g	880 cal/g	720 cal/cc	Not Stated
Company F - Region 2	Not Stated	0.82	831 cal/g	831 cal/g	681 cal/cc	Not Stated
Company G - Region 2	Not Stated	0.85	753 cal/cc, 866 cal/g	866 cal/g	753 cal/cc	Not Stated
Company H - Region 3	Not Stated	0.77 +/- 0.03	3.318 MJ/kg	912 cal/g	702 cal/cc	Not Stated
Company I - Region 3	Not Stated	0.80 +/- 0.05	746 cal/cc, 932 cal/g	932 cal/g	746 cal/cc	Not Stated
Company J - Region 4	Not Stated	0.75 - 0.82	2.26 MJ/kg	540 cal/g	424 cal/cc	Not Stated
ANFO - ISEE Handbook (1998)	Not Stated	0.82	3.75 MJ/kg	896 cal/g	734 cal/cc	101 MPa
ANFO - Atlas Handbook (1987)	Not Stated	0.81	3.816 MJ/kg	912 cal/g	739 cal/cc	Not Stated
ANFO - DuPont Handbook (1980)	Not Stated	0.80 - 0.85	900 cal/g	900 cal/g	742 cal/cc	Not Stated

Weight Strength (AWS), Absolute Bulk Strength (ABS), and density values used to define standard ANFO can vary among manufacturers. Handbooks published by manufacturers and professional societies also show variability. See Table 1 – Survey of standard ANFO values and ideal detonation codes.

Company propriety computer ideal detonation codes are often used to calculate and publish Relative Weight Strength (RWS) and Relative Bulk Strength (RBS) product energy values relative to their standard ANFO. The ideal energy values generated by these various computer codes while useful in comparing products within a given manufacturer's product line, often creates confusion for the end user when trying to cross compare published energy values between manufacturers.

Ideal detonation codes calculate explosive energies based on the inputs of the formulation composition and a database of theoretical thermodynamic properties for the various composites. Ideal detonation codes do not consider detonation efficiency realised through explosive material particle size and manufacturing refinement. As a simplified example, a given composition of salts, fuel, and water input into an ideal detonation code will produce the same energy values whether the raw materials are in solid blocks or highly processed. Likewise, ideal detonation codes do not calculate comparable energies realised by say a straight emulsion with highly refined particle versus a blend of 70% straight emulsion with highly refined particles blended with 30% AN/ANFO coarse grained particles.

Military, commercial, and academic institutions have continued to develop non-ideal detonation codes that strive to correct the shortcomings of calculations by ideal detonation codes. Non-ideal detonation codes are usually proprietary and once again generate values that are comparable only within the house running the code.

For the end user, it does raise the question of how does one go about understanding and comparing explosive energies between the different manufacturers?

Underwater bubble energy testing can be useful for making relative and comparable physical measurements of total, shock and gas energies realised by explosive products. UTEC Lab (Kansas, USA) is a reputable 3rd party explosives testing facility that may be engaged by manufacturers and end users to conduct underwater bubble energy, confined VOD testing, and other tests on commercial explosives. As an effort to understand and differentiate between various manufacturer explosive offerings, some major mining houses are now having manufacturers conduct and report physical measurements from UTEC as part of their tender process.

7 PHYSICAL TESTING AND EXPLOSIVE PERFORMANCE

Recent underwater bubble energy tests conducted at UTEC with single salt, dual salt and urea inhibited emulsions and emulsion blends record interesting differences in total energy, and shock and gas energy partitions between formulations.

Measurements from underwater bubble energy tests show the total energy difference on a volume basis (cal/cc) comparing a straight single salt AN emulsion to a straight dual salt ANCN emulsion is 1%, and the total energy difference on a weight basis (cal/g) is 2%. These measurements confirm the total energies realised by a straight dual salt ANCN emulsion is essentially equivalent to a straight single salt AN emulsion. The dual salt ANCN emulsion tested generated nearly equal amounts of shock and gas energies, while the

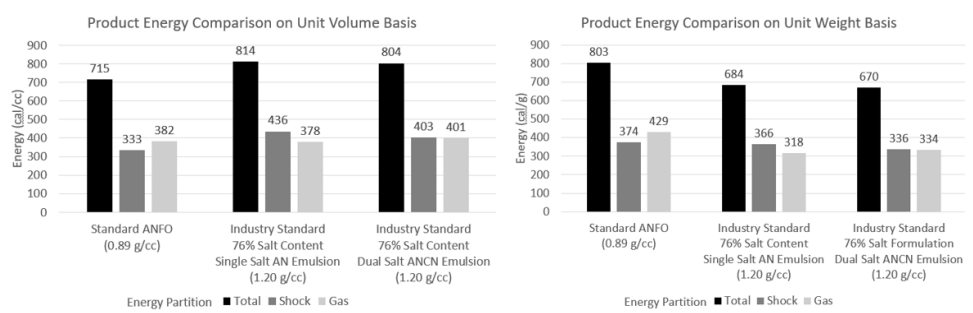

Figure 5. Underwater energy test measurements for straight single salt and dual salt emulsion.

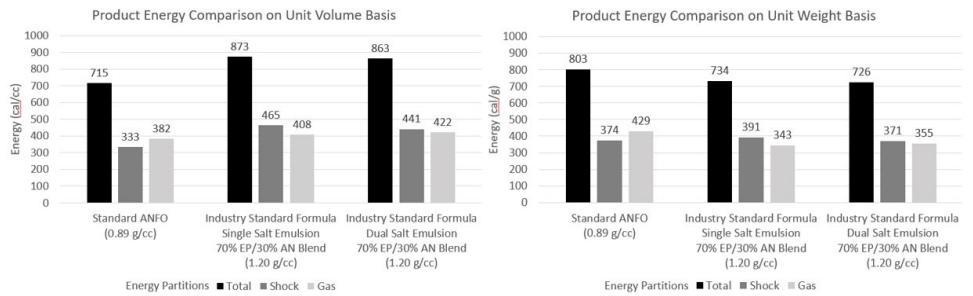

Figure 6. Underwater energy test measurements for single salt and dual salt emulsion blend.

single salt AN emulsion developed slightly greater shock energy and slightly less gas energy. See Figures 5 – Energy of straight single salt and straight dual salt emulsion.

Measurements from underwater bubble energy tests show the total energy difference on a volume basis (cal/cc) comparing a 70%EP/30% ANFO emulsion blend made with single salt AN emulsion blend and a dual salt ANCN emulsion blend is 1%, and the total energy difference on a weight basis (cal/g) is also 1%. These measurements confirm the total energies realised by a dual salt ANCN emulsion blend is essentially equivalent to a single salt AN emulsion blend. The dual salt ANCN emulsion blend tested generated slightly greater gas energy as compared to the single salt AN emulsion blend. See Figures 6 – Energy of single salt and dual salt emulsion blend.

8 REACTIVE GROUND INHIBITION BY UREA

Urea is a nitrogen rich organic chemical compound that is not a salt. While not a salt, urea has won its place in bulk emulsion explosive formations as the most effective chemical inhibitor in explosives that contain ammonium nitrate (AN) against reactive ground. Urea inhibits the exothermic reactive ground chain of reaction by trapping the vital catalyst nitrous acid. See Equation 4, Urea-nitrous acid inhibition.

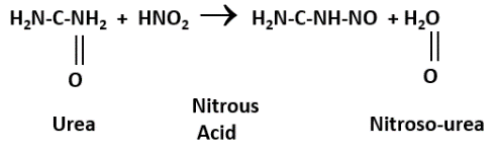

Equation 4.

Urea is an inhibiting agent only and it does get consumed, and possibly exhausted, during exposure to reactive ground and the inhibition process. Accordingly, it is extremely important to have urea inhibited emulsion formulations qualified for use in reactive ground by isothermal testing. Isothermal testing provides an understanding of how resistant an inhibited AN based explosive product is to onset reaction and the duration of the safe loading window before the inhibition is no longer effective.

Urea inhibition incrementally reduces energy release and sensitivity. Most mild to moderately reactive grounds may be managed with 3% to 6% urea inhibition. Highly reactive ground may

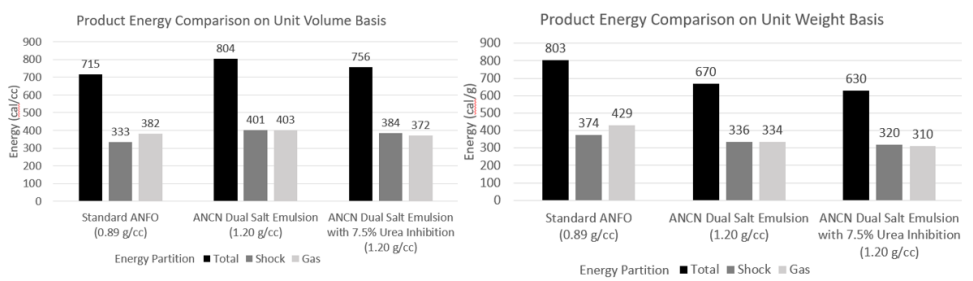

Figure 7. Underwater energy test measurements for dual salt emulsions w/wo urea inhibition.

require urea inhibition up to 10%. To ensure reliable initiation with primers assemblies made using standard detonators or detonating cord and/or cast primers or detonator sensitive emulsions, the urea content in inhibited emulsions typically is usually no more than 10% of the total formulation. Understanding the urea content of an inhibited product is important when comparing the energies of inhibited emulsion products. See Figure 7, energy of dual salt emulsions with and without urea inhibition.

There is a considerable amount of public knowledge available describing explosives and blasting applications in reactive ground types for those interested or needing it.

9 CONCLUSIONS

The purpose of this paper has been to acquaint blasting professionals with bulk emulsions and emulsion blends formulated with single salt, dual salts, and multiple salts.

Summary of key takeaways and learnings for the reader:

- Product stability. Dual and multiple salt emulsions are inherently chemically resistant to crystallisation and phase separation. Emulsion stability should be considered when risk assessing product selection for transportation survivability, resistance to breakdown by repeated re-pumping, and salting out during extended storage times.
- In using gassed emulsions and emulsion blends, the maximum hole depth loaded depends on product selection, hole diameter, product densities, critical void space and the presence of water. End users should consult manufacturer specialists for additional guidance and site-specific calculations before loading holes to ensure reliable application.
- Environmental considerations. Dual salt ANCN emulsions require less energy intensity to manufacture as compared to single salt AN emulsions. Dual salt ANCN emulsions formulations are closely oxygen balanced and realise minimise generation of post blast NOx. Dual salt ANCN salt emulsions formulations can significantly reduce the concentration of toxic ammonia in mine-water thus reduce the amount of treatment mine-water requires before release to the environment. With concern to nitrates in mine-water, dual salt ANCN emulsions do not offer any advantage over a single salt AN emulsion.
- Energy values (RWS and RBS) generated by manufacturer ideal detonations codes vary from code to code. Energy values for products stated by a manufacturer are directly comparable to only to formulations and products made by that manufacturer. Directly comparing published energy values (RWS and RBS) between different manufacturers may not be completely meaningful.
- Physical testing by underwater bubble energy tests confirm that single salt (AN) emulsions and dual salt (ANCN) emulsions produce similar bulk and volumetric energies, and comparable gas and shock energy partitions.
- Urea is the most effective chemical inhibitor for AN based explosives against reactive ground. Urea inhibited emulsion realise reduced energy as compared to their non-inhibited counterparts.

People interested in expanding their knowledge on any one of the topics presented in this paper are highly encouraged to explore the public domain and interact with other experienced chemists, researchers, and end users.

10 ACKNOWLEDGEMENTS

The authors appreciate the support and efforts of all BME personnel that contributed to building the body of knowledge hosted in this paper. The authors also express gratitude to the explosive physical testing professionals at UTEC Corporation, R&D Lab for their all support over the past several years. Special thanks to Gary Eck, Special Project Manager for being our key contact.

REFERENCES

Alleman, J.E. 1998. Free Ammonia-Nitrogen Calculator & Information.https://www. http://home.eng.iastate.edu/~jea/w3-research/free-ammonia/nh3.html

Atlas Power Company Basic Technical Training, circa mid-1980s.

Oluwoye, I., Dlugogorski, B.Z., Gore, J., Oskierski, H.C., & Altarawneh, M. 2017. Atmospheric emission of NO*x* from mining explosives: A critical review, *Atmospheric Environment* (2017), doi: 10.1016/j.atmosenv.2017.08.006.

Unpublished internal reports. UTEC Corporation, R&D Laboratory. BME Underwater Anergy and Confined VOD testing results. 2018, 2019, and 2020.